SPECIAL REPORT 122

DRAG AND PROPULSIVE CHARACTERISTICS OF AIR-COOLED ENGINE-NACELLE INSTALLATIONS FOR LARGE AIRPLANES

By Abe Silverstein and Herbert A. Wilson, Jr.
Langley Memorial Aeronautical Laboratory

August 1939

DRAG AND PROPULSIVE CHARACTERISTICS OF AIR-COOLED ENGINE-NACELLE INSTALLATIONS FOR LARGE AIRPLANES

By Abe Silverstein and Herbert A. Wilson, Jr.

SUMMARY

An investigation is in progress in the N.A.C.A. full-scale wind tunnel to determine the drag and the propulsive efficiency of nacelle-propeller arrangements for a large range of nacelle sizes. In contrast with the usual tests with a single nacelle, these tests were conducted with nacelle-propeller installations on a large model of a 4-engine airplane. Data are presented on the first part of the investigation, covering seven nacelle arrangements with nacelle diameters from 0.53 to 1.5 times the wing thickness. These ratios are similar to those occurring on airplanes weighing from about 20 to 100 tons.

The results show the drag, the propulsive efficiency, and the over-all efficiency of the various nacelle arrangements as functions of the nacelle size, the propeller position, and the airplane lift coefficient. The effect of the nacelles on the aerodynamic characteristics of the model are shown for both propeller-removed and propeller-operating conditions.

INTRODUCTION

The trend toward increasing airplane size unaccompanied by a corresponding increase in the diameter of air-cooled engines has led to designs in which the engine-nacelle diameter is equal to, or even less than, the wing thickness. In contrast, the engine-nacelle diameter for small high-performance airplanes is from four to five times the wing thickness. Data on nacelle installations are available chiefly in the range of the ratio of nacelle diameter to wing thickness from 1.5 to 2.0. In order to investigate more completely the entire range, tests are being conducted in the N.A.C.A. full-scale wind tunnel for ratios of nacelle diameter to wing thickness varying from 0.53 to 4.0. This paper presents the results obtained for the smaller nacelles with diameters varying from 0.53 to 1.5 times the wing thickness.

In contrast with the usual tests of a single nacelle, this investigation has been made with four nacelles on

a midwing monoplane model simulating a modern 4-engine airplane. By this method, not only was the drag measured with greater certainty but also the effects of the nacelles and the propeller slipstream on the airplane characteristics were determined. Nacelles of three diameters were tested, each for several positions of the propeller ahead of the wing leading edge. The 4-engine model with the nacelles of different size may be considered to represent airplanes of different size; the model with the largest nacelle may simulate a 20-ton airplane, and the model with the smallest nacelle may simulate one of about 100 tons.

SYMBOLS

α, angle of attack of the fuselage reference axis relative to the wind axis, degrees.

q, dynamic pressure, pounds per square foot.

S, wing area, square feet.

$\bar{c}$, mean chord of the wing, area/span, feet.

t_w, maximum wing thickness (average for the two lateral nacelle locations), feet.

D_p, propeller diameter, feet.

D_N, maximum nacelle diameter, feet.

F, maximum cross-sectional area of nacelle, square feet.

V, air speed, feet per second.

L, lift, or force normal to the relative wind, pounds.

D, drag, or force parallel to the relative wind, pounds.

D_c, power-off drag of model with engine-nacelle installation, pounds.

M, pitching moment, pound-feet.

$C_L = L/qS$

$C_D = D/qS$ (Subscript w refers to power-off drag of the model with bare wing; subscript c, to power-off drag of the model with engine-nacelle installation.)

$\Delta C_D = C_{D_c} - C_{D_w}$

$C_{D_F} = \frac{\Delta C_D S}{4F}$

$C_m = M/qS\bar{c}$

R, resultant force of a propeller-nacelle-wing combination, pounds.

T, thrust of propellers operating in front of a body (tension in propeller shafts), pounds.

ΔD, increase in drag of the body due to the action of the propellers, pounds.

$T - \Delta D$, effective thrust of the propeller-nacelle installation.

T_o, index thrust.

P, power input to all propellers.

$\eta = \frac{(T - \Delta D)V}{P}$, propulsive efficiency.

$\eta_t = \eta(C_{D_w}/C_{D_c})$, over-all efficiency.

$T_{c_o}' = \frac{P\eta_o}{\frac{1}{2}\rho V^3 S}$, index thrust coefficient.

$\eta_o = \eta$ at $C_L = 0.25$.

n, propeller speed, revolutions per second.

β, propeller blade angle at 0.75 radius, degrees.

δ_f, flap deflection from closed position, degrees.

MODEL AND TEST EQUIPMENT

The tests were conducted in the N.A.C.A. full-scale wind tunnel, which is described in reference 1. The model is a metal-covered, midwing monoplane with a span of 37.25 feet. The symmetrical wing sections are tapered in thickness from the N.A.C.A. 0018 at the root to the N.A.C.A. 0010 at the tip. The wing plan form tapers 4:1 from a root chord of 7.28 feet, and the wing area is 172 square feet. Split trailing-edge flaps with an average chord of 0.15c extend over the middle 60 percent of the span with the exception of a short gap at the fuselage. The angle of wing setting to the fuselage reference line is 4.6°. The principal dimensions of the model and the nacelle for each of the test arrangements are shown in figure 1. Figures 2 to 5 show the model installed in the full-scale tunnel.

A summary of the nacelle installations investigated is shown in table I.

TABLE I

Test	Nacelle diameter (in.)	$\frac{D_N}{t_w}$ (1)	Propeller diameter (in.)	Propeller location (2)	Details in
1	No cowling - Bare-wing model				fig. 2
2a	20	1.50	39	0.40c	fig. 1(c)
2b	20	1.50	39	.25c	fig. 5
3a	10.4	.78	39	.40c	fig. 4
3b	10.4	.78	39	.25c	fig. 1(b)
4a	7	.53	24	.40c	fig. 1(a)
4b	7	.53	24	.25c	fig. 1(a)
4c	7	.53	24	.13c	fig. 3

[1] Thickness t_w is the average of wing thicknesses at the nacelle locations.

[2] Chord c is the local chord at each propeller location.

Four 3-blade metal propellers of 39-inch diameter were used for the tests with the nacelles 20 and 10.4 inches in diameter. Blade dimensions and sections for the propeller are given in figure 6. Four 2-blade metal propellers of 24-inch diameter and Navy 4412 design were used for the tests with the 7-inch nacelles. The propellers were driven, through extension shafts, by 25-horsepower alternating-current motors enclosed within the wing. The speed of the propellers was regulated by varying the frequency of the motor-current supply and was measured with an electric tachometer. The propeller torques were determined from an electric calibration of the motors.

Figure 7 is a diagram of a representative cowling-nacelle installation, with the dimensions for the cowling given as fractions of the cowling diameter. The cowling was geometrically similar to the one designated cowling C in reference 2. Perforated metal plates were used to furnish a resistance similar to that of a well-baffled engine. The number of holes in the plates was adjusted to give a value of conductivity K (reference 3) of approximately 0.10. The exit slot of the cowling was proportioned to provide a pressure drop across the engine of 0.35q, corresponding to sufficient cooling for flight at 200 miles per hour; it is assumed that cowling flaps or other adjustments will be provided for different flight conditions. Smooth fairing of the nacelles into the wing was provided by small fillets at the junctures of the wing and the nacelles (figs. 3, 4, and 5). In order to change the propeller position from 0.25c to 0.40c, the nacelle was extended by inserting a cylindrical section at A (fig. 7). For the tests with no cooling air, the perforations in the metal plates were sealed. For the tests of the 7-inch nacelles, no provision was made for the flow of cooling air through the cowling, because it was anticipated that the effects of cooling-air flow would not be measurable for this arrangement.

TESTS

With the propellers removed from the model, measurements of aerodynamic forces and pitching moment were made at an air speed of about 60 miles per hour for all the nacelle installations over an angle-of-attack range from zero lift through the stall. Scale effect on the drag at low lift coefficients was also measured over a range of air speeds from 30 to 100 miles per hour.

With the propellers operating, propulsive characteristics of the nacelle-propeller installations were determined for the attitude in which the thrust axes were parallel to the relative wind and for lift coefficients approximating those for high-speed and climbing flight. In addition to the usual aerodynamic forces and pitching moment, the power-on measurements included the power input to the propellers and the propeller speed. The procedure followed in the propeller tests was to hold the torque constant and to increase the tunnel air speed in steps from 30 to 100 miles per hour, after which the propeller speed was reduced until zero thrust was reached. The effect of the propeller operation upon the lift and the pitching moment was determined at a tunnel speed of approximately 60 miles per hour for several thrust conditions and with the propellers freewheeling.

The conductivity of the perforated cowling plate and the air flow through the cowling were determined from measurements of the pressure drop across the plate and of the dynamic and the static pressures at the cowling exit.

POWER-OFF CHARACTERISTICS

The aerodynamic characteristics of the 4-engine model with the propeller removed are shown in figures 8 to 15 for the various arrangements tested. These data were obtained at a tunnel air speed of about 60 miles per hour, which corresponds to a Reynolds Number of 2,500,000 based on the average wing chord of 4.62 feet. The coefficients are based on a wing area of 172 square feet and are corrected for wind-tunnel effects. Pitching-moment coefficients are computed about a center of gravity located as shown in figure 1. The tests were made with cooling air flowing through the cowling corresponding to that required for high-speed flight.

Drag.- Scale effects on the airplane drag coefficients for the nacelle arrangements tested are shown in figure 16 at the assumed high-speed lift coefficient of 0.25. Reference curves showing the scale effects on the model without nacelles are shown in figure 17 for values of C_L from -0.2 to 0.7.

At low lift coefficients, the curves of figures 16 and 17 show the negative-slope characteristics of plots of skin-

friction drag coefficient against Reynolds Number. At high lift coefficients, where the skin friction is only a small part of the total drag, the drag coefficient is about the same over the range of velocities tested. This result, which is also representative of the various cowling installations, is shown in figure 17 for the bare-wing model. Particularly interesting is the fact that the increment of drag due to the nacelle installations is essentially independent of the test velocity.

The increments of the airplane drag coefficient ΔC_D due to the presence of four nacelles are plotted against the ratio of the nacelle diameter to the wing thickness in figure 18. These increments are given for several lift coefficients, both with air flowing through the cowling (fig. 18(a)) and with the cowling closed (fig. 18(b)). The values were taken from the scale-effect curves (fig. 16) at a test velocity of 100 miles per hour.

If the nacelle drag increments for the cases of no air flow and with an air flow sufficient for cooling in high-speed flight are compared, it is noted that the effect of the air flow on the drag coefficient is slight. This result has been noted in previous investigations in which the cooling-air flow was properly regulated (reference 4). At the higher lift coefficients, in some cases, the drag was reduced by the air flow through the cowling.

In order to demonstrate the magnitude of the nacelle drag for airplanes of different size, it will be assumed that the drag coefficient of an efficient airplane without nacelles is 0.015 at a high-speed lift coefficient of 0.15. For a 75-ton airplane in which the ratios of D_N/t_w may be about 0.6, the increment of drag coefficient due to four nacelles with propellers at the 0.25c location (fig. 18(a)) is 0.0005. Further, if a 6-engine installation for an airplane of this size is assumed, the drag coefficient of the nacelles is 0.00075, or 5 percent of the total airplane drag.

For another typical design of a 20-ton, 4-engine airplane, the ratio of D_N/t_w may be 1.5 so that, by interpolation of figure 18(a), $\Delta C_D = 0.0036$ at $C_L = 0.15$. In this case, the drag of the nacelles is 24 percent of the total airplane drag. The relatively greater adverse effect of the large nacelles on the smaller airplane is clearly demonstrated.

The drag increments ΔC_D of figure 18 are presented in figure 19 in the form of C_{D_F}, which is the drag coefficient for a single nacelle based on the maximum cross-sectional area of the nacelle. The curves of figure 19 are of particular interest in pointing out the relatively larger nacelle drag coefficients of the small nacelles at the high lift coefficients and the lower drag of the shorter nacelles at low lift coefficients.

It is believed that the prediction of nacelle drag over the range of nacelle sizes tested can be made with considerable accuracy by reference to figure 19. The change in drag for cooling flows different from the ones tested in this investigation can be computed by the method of reference 4.

Lift.- The addition of nacelles to the airplane tends to increase slightly the slope of the lift curve, the increase being about proportional to the nacelle size (figs. 8 to 15). The lift-curve slope was increased about $2\frac{1}{2}$ percent by the four 20-inch nacelles. The higher lift is attributed to the increased area added by the nacelles and is consistent with results of previous investigations. The angle of zero lift was also slightly changed by the nacelles, the difference being about 0.2° for the 20-inch nacelles.

The maximum lift coefficient of the airplane with cooling air flowing through the cowling varied with the nacelle installation, as shown in table II.

TABLE II

Values of Maximum Lift Coefficient

$\frac{D_N}{t_w}$	Propeller location	Flap deflection, δ_f	
		0°	60°
Without nacelles		1.31	--
0.53	0.13c	1.33	1.83
.53	.25c	1.35	1.83
.53	.40c	1.32	1.81
.78	.25c	1.37	1.77
.78	.40c	1.36	1.80
1.50	.25c	1.21	1.65
1.50	.40c	1.17	1.60

In comparison with the maximum lift coefficient of the model without nacelles, the model with the small nacelles has slightly higher values and the model with the large nacelles has considerably lower values. The large decreases in maximum lift coefficient for the installations with nacelle diameters larger than the wing thickness are attributed to different pressure distributions over the upper surface of the nacelle and the adjacent wing surface. Tuft observations (fig. 20) on the upper surface of the airfoil near the rear of the large nacelles at high lift coefficients show the flow spreading out laterally on both sides of the nacelle. This result indicates a higher pressure on the nacelle than on the adjacent wing surface, owing to the expansion of the air behind the maximum nacelle section.

The lateral motion of the air in the region of adverse pressure gradient on the wing has a strong destabilizing effect and causes breakdown of the flow. In the case of the cowling with $D_N/t_w = 1.5$, the maximum lift was decreased about 9 percent. For an unpublished case of a cowling installation with $D_N/t_w = 3.7$, the $C_{L_{max}}$ was

decreased 16.5 percent. In case the nacelle diameter is about equal to or less than the wing thickness, the nacelle does not extend into the region of adverse pressure gradient on the wing and there is no large taper to the nacelle with the attendant adverse pressure gradient. The slight increase in $C_{L_{max}}$ shown by the small nacelles is attributed to the increased surface area of the wing-nacelle combination.

Lift-drag ratio.- Since the range of an airplane is about proportional to the value of the maximum lift-drag ratio, the large reductions in its value caused by even the smallest nacelles should be pointed out. In comparison with the assumed case of an airplane without nacelles, the smallest nacelle installation ($D_N/t_w = 0.53$) reduced the value of $(L/D)_{max}$ by about 14 percent (fig. 21); whereas the large nacelles reduced it by about 25 percent. Based on these power-off data, the large nacelles with propellers at 0.40c ahead of the wing are indicated to be inferior to the shorter nacelles. The results of figure 21 substantiate those of figure 19 in showing that the small nacelles contribute considerably more drag at the high than at the low lift coefficients. The lift coefficient for the maximum lift-drag ratio for the model is about 0.55.

Pitching moment.- The large nacelles have a marked destabilizing effect on the airplane. This result is shown in figure 22, in which the slopes of curves of the pitching-moment coefficient are plotted against nacelle size. The slopes shown in figure 22 were taken over the straight portions of the pitching-moment curves between $\alpha = -5^\circ$ and 5°; the decreased stability is indicated by the lower values of the negative slope. The slope of the pitching-moment curve is decreased by the nacelles even more markedly at high angles of attack, as shown by noting the slopes on figures 8 and 9 between $\alpha = 8^\circ$ and 12°. The decrease of the slope of the pitching-moment curve is attributed to a forward movement of the aerodynamic center of the wing due to the addition of the nacelle surface ahead of the leading edge.

This reasoning is substantiated by figure 22, in which it may be noted that the longer nacelles show the greater destabilizing effects. At the high angles of attack, the resultant force on the cowling contributes a large positive moment and, unless this effect is taken into consideration in the tail-plane design, it may lead to instability.

PROPULSIVE AND OVER-ALL EFFICIENCIES

The nacelle drag coefficients alone are not a sufficient basis for comparison of the various nacelle-propeller installations. The installations are more properly compared by means of an over-all efficiency that includes the nacelle-drag increment measured with the propellers removed as well as the propulsive efficiency. This over-all efficiency η_t is defined as the ratio of the tow-line power required for the bare-wing model (without nacelles) at a given level-flight speed to the actual power input required at this speed by the model with the nacelle-propeller installations. In this method, the over-all efficiency of the bare-wing model is 100 percent and, for a nacelle-propeller installation, it is given by

$$\eta_t = \eta \, (C_{D_w}/C_{D_c})$$

The propulsive efficiency η is the ratio of the effective thrust power to the power input and may be calculated from the relation

$$\eta = \frac{(T - \Delta D)\, V}{P}$$

The value of the effective thrust, $T - \Delta D$, may be computed from the wind-tunnel data by means of the relation

$$T - \Delta D = D_c + R$$

in which D_c and R are the observed readings on the drag scale for propeller-removed and propeller-operating conditions, respectively.

For tests without a lifting surface behind the propeller, $T - \Delta D$ may be calculated from measurements of D_c and R obtained at the same angle of attack and dynamic pressure. When the flow over a lifting surface is influenced by the propeller, the changes in lift as well as in drag should be credited to or charged against the propeller. The change in lift has been allowed for in these results by making measurements of D_c and R at the same lift coefficient instead of at the same angle of attack.

Propulsive Efficiencies

Data have been obtained to show the effect on the propulsive efficiency of variations in the following:

1. Propeller blade angle.
2. Nacelle diameter.
3. Propeller location.
4. Air flow through cowling.
5. Lift coefficient.

Propeller blade angle.- The results obtained with the 39-inch-diameter 3-blade propellers (figs. 23 to 26) are consistent in indicating that the maximum propulsive efficiency occurs at a blade angle β of about 30°. The envelopes of the efficiency curves are flat, however, and variation in β of $\pm 8^\circ$ from the optimum causes only slight reductions in η_{max}. The 2-blade propeller used with the small nacelles also shows maximum efficiency at $\beta = 30^\circ$ (figs. 27 to 29). The envelopes are not flat, and slight variations from the optimum blade angle lead to substantial decreases in η_{max}.

From analysis of figures 23 to 29, it may be concluded that the blade angle for maximum propulsive efficiency is not greatly affected by the location of the propeller with reference to the wing or by the diameter of the nacelle behind the propeller.

Nacelle diameter.- The effect of variation in the nacelle diameter on the maximum propulsive efficiency is shown by a comparison of figures 23 and 24 with figures 25 and 26. For each propeller location, the smaller of the two nacelles shows a slightly lower propulsive efficiency. This difference, however, does not exceed 1 percent, which is about the experimental accuracy of the measurements. The results of these tests indicate, in the usual range, that the propulsive efficiency is almost independent of the ratio of the propeller to the cowling diameter. It should be noted that the value of zero propulsive efficiency, that is, zero effective thrust, occurs at higher values of V/nD for the large nacelle than for the small one.

Propeller location.- The variation of the propulsive efficiency with propeller location for the 3-blade propeller installations is shown by comparing figures 23 and 25 with figures 24 and 26. The propeller on the 20-inch nacelles ($D_N/t_w = 1.5$) shows about the same maximum efficiency with the propeller located in either the 0.40c or the 0.25c position. The installation with the 10.4-inch nacelles ($D_N/t_w = 0.78$) shows a slightly higher maximum efficiency with the propeller in the 0.25c position, but the differences are only slightly greater than the experimental accuracy.

The two-blade propeller on the 7-inch-diameter nacelle installation was tested 0.40c, 0.25c, and 0.13c ahead of the wing leading edge. The results (figs. 27 to 29) show the 0.25c location to be the most favorable, with the propulsive efficiency 2 percent higher than for the 0.40c location and 3.5 percent higher than for the 0.13c location. The results are of interest in demonstrating that, although from structural considerations it may be desirable on large airplanes to place the propeller close to the wing leading edge, the position is aerodynamically inferior.

Air flow through cowling.- The effect on the propulsive efficiency of air flow through the cowling corresponding to that required for cooling at high-speed flight is shown by comparison of figures 23 to 26 with figures 30 to 33. The 10.4-inch nacelles show the same maximum efficiencies with and without air flowing. The large nacelles rather consistently show maximum efficiencies about 1 percent higher for the closed cowlings than for the open ones.

These results indicate that the propulsive efficiencies measured on nacelle installations with no air flowing through the cowling are sufficiently accurate for predicting the values that will be obtained with correct cooling flow. Other nacelle tests with excessive cooling air and poorly designed cowling outlets do not substantiate this conclusion.

Lift coefficient.- The variations in the propulsive efficiencies with airplane lift coefficient are shown in figures 34 to 37. The results are shown for $\beta = 23\frac{1}{2}^{\circ}$, which was chosen as an average flight propeller setting for the range of lift coefficients tested. In each case, the maximum propulsive efficiency was obtained at $C_L = 0.70$ and the lowest at $C_L = .0.25$, with an average

difference between them of about 4 percent. The high efficiency at $C_L = 0.70$ is due to the favorable effect of the propeller slipstream in decreasing the interference between the nacelle and the wing. The presence of this interference and its effect in increasing the value of C_{D_F} at the higher lift coefficient has previously been noted.

The propulsive efficiency for $C_L = -0.04$, in which case the nacelle axis was parallel to the relative wind, was higher than for the high-speed flight condition $C_L = 0.25$.

Over-All Efficiency

As mentioned previously, neither the nacelle drag coefficient C_{D_F} nor the propulsive efficiency η alone is a sufficient measure of the efficiency of the conversion of engine power into the power available for propelling the airplane. A propulsion system should be credited only with the power available to pull the airplane minus the power plant through the air. Values of maximum over-all efficiency for propeller locations at 0.25c are plotted in figure 38 against nacelle size and an almost linear relation is shown. It is of importance to note that, for the nacelle with $D_N/t_w = 1.5$, only about two-thirds of the engine power is usefully employed.

The variation in maximum over-all efficiency with lift coefficient is shown in figure 39 for the 10.4-inch and the 20-inch nacelles. The over-all efficiency is highest with the nacelle axis parallel to the relative wind ($C_L = -0.04$) and lowest at the high-speed lift coefficient. The efficiencies for the 0.25c and 0.40c propeller locations are similar, with a slight superiority indicated for the 0.25c location with the smaller nacelle. The comparison given in figure 39 is made for $\beta = 23\frac{1}{2}^\circ$ and is slightly unfair at $C_L = 0.25$ to the 20-inch nacelle with propeller at 0.25c. This installation has a maximum efficiency at a somewhat higher blade angle and, if the comparison had been made for this condition, the values for the 0.25c and 0.40c propeller locations would have been in essential agreement. On the basis of over-all efficiencies, it may be concluded that the 0.25c location is most favorable for the small nacelles and, for the 20-inch nacelles, the 0.25c and 0.40c propeller locations are of equal merit.

POWER-ON CHARACTERISTICS

The effect of propeller operation on the aerodynamic characteristics of an airplane is primarily dependent on the amount of thrust delivered by the propellers and, for a given thrust, is relatively independent of moderate changes in blade angle, V/nD, propulsive efficiency, and propeller diameter. In order to describe the conditions of propeller operation, use is made of an index thrust coefficient which takes the form

$$T_{c_o}' = \frac{T_o}{qS} = \frac{P\eta_o}{qSV}$$

in which η_o is the propulsive efficiency at $C_L = 0.25$ for the conditions of V/nD and blade angle at which the tests were made. The index thrust coefficient has the characteristics and form of a drag coefficient and is essentially independent of the combination of V/nD and blade angle that produces the thrust; it is exactly equal to the amount of drag that the thrust would counterbalance at the standard or index condition and, at any other value of lift coefficient, differs from the true thrust coefficient only by the variation in propulsive efficiency between the two conditions.

The effect of propeller operation on the lift of the model is shown in figures 40 to 42 for three of the nacelle installations. Results are given for the conditions of flap neutral and flap deflected 60°.

For the model with flaps neutral, the effect of the propeller operation in each case is to increase slightly the slope of the lift curve and to increase greatly the maximum lift coefficient. With the flaps deflected, the slope of the lift curve and the maximum lift coefficient are not so greatly increased by the propeller operation. With increasing values of T_{c_o}', the maximum lift with flaps up approaches that for the flaps-down condition. The large increase in the maximum lift coefficient between the propeller-off condition and the power-on condition with $T_{c_o}' = 0.1$ (fig. 40) is due to the effect of the slipstream in decreasing the wing-nacelle interference. The maximum lift coefficients determined with freewheeling propellers were about the same as those for the propeller-off condition.

The large increase in maximum lift due to the propeller operation with the small propellers and nacelles (fig. 42) is striking. The low test values of T_{c_o}' for this case are due to the lower power input required by the small-diameter propellers; it should be pointed out that the slipstream velocity for $T_{c_o}' = 0.1$, with the small 24-inch propellers, is actually similar to that for $T_{c_o}' = 0.3$ in the case of the 39-inch propellers. The wing area immersed in the slipstream of the small propellers is only about 0.6 as much as for the large propellers and a corresponding decrease in slipstream effect would normally be expected. This subject should receive further study.

The effects of the propeller operation on the pitching-moment coefficient, for the various thrust coefficients and nacelle installations, are shown in figures 43 to 45. With the flap neutral, the principal effect of the propeller operation is to change the elevator angle required for balance. The pitching-moment curves are of similar shape and, except in the negative angle-of-attack range, the curves are similar to the ones that might be obtained by a shift of the tail angle. With the flaps deflected, the slope of the pitching-moment curve is greatly decreased with increasing thrust so that, for extreme conditions (fig. 43 at $T_{c_o}' = 0.3$), instability is indicated over a considerable range of angles of attack. The pitching-moment curves for the 20-inch and 10.4-inch nacelle installations, although similar in shape and general characteristics, are somewhat different in numerical values. The small nacelle installation, which was tested with the 24-inch-diameter propellers, shows smaller effects of the power on the moment although, in general, the effects are similar to those for the large nacelle.

CONCLUSIONS

1. The over-all efficiency of propulsion of the 4-engine model at conditions of high-speed flight decreased linearly from about 77 to 67 percent as the nacelle diameter was increased from 0.5 to 1.5 times the wing thickness.

2. Nacelle installations with the propeller located

0.25c ahead of the leading edge were superior to those having the propeller at the 0.40c location in the range of ratios of nacelle diameter to wing thickness from about 0.5 to 1. For a value of the ratio of nacelle diameter to wing thickness of 1.5, the 0.25c and the 0.40c propeller locations were of about equal merit. The propulsive efficiencies for small nacelle-propeller installations close to the leading edge of a wing were lower than for the 0.25c location.

3. The propulsive efficiency of the 39-inch-diameter propeller was about the same for tests made with the 10.4-inch and the 20-inch nacelles.

4. The values of propulsive efficiency determined with or without air flow through the cowling were in substantial agreement.

5. The maximum lift-drag ratio of the model was substantially reduced by nacelles even of very small ratios of nacelle diameter to wing thickness.

6. The nacelle installations contributed destabilizing moments to the airplane that must be considered in the tail design.

7. The power-off maximum lift coefficient of the airplane was decreased about 9 percent for the nacelle installation having a value of the ratio of nacelle diameter to wing thickness of 1.5 and was slightly increased by small nacelles.

Langley Memorial Aeronautical Laboratory,
National Advisory Committee for Aeronautics,
Langley Field, Va., May 17, 1939.

REFERENCES

1. DeFrance, Smith J.: The N.A.C.A. Full-Scale Wind Tunnel. T.R. No. 459, N.A.C.A., 1933.

2. Robinson, Russell G., and Becker, John V.: High-Speed Tests of Radial-Engine Cowlings. T.R. (to be published), N.A.C.A., 1939.

3. Theodorsen, Theodore, Brevoort, M. J., and Stickle, George W.: Full-Scale Tests of N.A.C.A. Cowlings. T.R. No. 592, N.A.C.A., 1937.

4. Stickle, George W.: Design of N.A.C.A. Cowlings for Radial Air-Cooled Engines. T.R. No. 662, N.A.C.A., 1939.

FIGURE LEGENDS

(a) The 7-inch nacelles; $D_N/t_w = 0.53$
(b) The 10.4-inch nacelles; $D_N/t_w = 0.78$.
(c) The 20-inch nacelles; $D_N/t_w = 1.5$.

Figure 1.- Diagram of model showing arrangements of the nacelles.

Figure 2.- Installation of model without nacelles in the N.A.C.A. full-scale wind tunnel.

Figure 3.- Installation of model with 7-inch nacelles and 0.13c propeller location in the N.A.C.A. full-scale wind tunnel.

Figure 4.- Installation of model with 10.4-inch nacelles and 0.40c propeller location in the N.A.C.A. full-scale wind tunnel.

Figure 5.- Installation of model with 20-inch nacelles and 0.25c propeller location in the N.A.C.A. full-scale wind tunnel.

Figure 6.- Blade dimensions for 3-blade model propellers. All linear dimensions given in inches.

Cowling profile

x/D_N	y/D_N	x/D_N	y/D_N
0	0.350	0.115	0.460
.005	.378	.135	.467
.010	.387	.154	.474
.019	.399	.192	.485
.038	.416	.231	.493
.058	.431	.269	.498
.077	.441	.308	.500
.096	.452	.335	.500

Figure 7.- Dimensions of cowling and cowling arrangement.

Figure 8.- Aerodynamic characteristics of model without nacelles.

Figure 9.- Aerodynamic characteristics of model with 20-inch nacelles and 0.40c propeller location.

Figure 10.- Aerodynamic characteristics of model with 20-inch nacelles and 0.25c propeller location.

Figure 11.- Aerodynamic characteristics of model with 10.4-inch nacelles and 0.40c propeller location.

Figure 12.- Aerodynamic characteristics of model with 10.4-inch nacelles and 0.25c propeller location.

Figure 13.- Aerodynamic characteristics of model with 7-inch nacelles and 0.40c propeller location.

Figure 14.- Aerodynamic characteristics of model with 7-inch nacelles and 0.25c propeller location.

Figure 15.- Aerodynamic characteristics of model with 7-inch nacelles and 0.13c propeller location.

(a) Air flowing through cowling.
(b) Cowling closed.

Figure 16.- Scale effect on drag coefficient at $C_L = 0.25$.

Figure 17.- Scale effect on the model without nacelles for the range of lift coefficients.

(a) Air flowing through cowling.
(b) Cowling closed.

Figure 18.- Drag increments due to nacelles for various size nacelles and lift coefficients.

(a) Air flowing through cowling.
(b) Cowling closed.

Figure 19.- Nacelle drag coefficient for various size nacelles and lift coefficients.

Figure 20.- Air flow over upper surface of wing and nacelle. The 20-inch nacelle; 0.25c propeller location; α, 12°.

Figure 21.- Variation of the maximum lift-drag ratio of the model for various nacelle sizes.

Figure 22.- Variation of the slope of the pitching-moment curve of the model for various nacelle sizes.

Figure 23.- Variation of propulsive efficiency with blade angle. The 20-inch nacelles; 0.40c propeller location; C_L, 0.25; air flowing through cowling.

Figure 24.- Variation of propulsive efficiency with blade angle. The 20-inch nacelles; 0.25c propeller location; C_L, 0.25; air flowing through cowling.

Figure 25.- Variation of propulsive efficiency with blade angle. The 10.4-inch nacelles; 0.40c propeller location; C_L, 0.25; air flowing through cowling.

Figure 26.- Variation of propulsive efficiency with blade angle. The 10.4-inch nacelles; 0.25c propeller location; C_L, 0.25; air flowing through cowling.

Figure 27.- Variation of propulsive efficiency with blade angle. The 7-inch nacelles; 0.40c propeller location; C_L, 0.25; cowling closed.

Figure 28.- Variation of propulsive efficiency with blade angle. The 7-inch nacelles; 0.25c propeller location; C_L, 0.25; cowling closed.

Figure 29.- Variation of propulsive efficiency with blade angle. The 7-inch nacelles; 0.13c propeller location; C_L, 0.25; cowling closed.

Figure 30.- Variation of propulsive efficiency with blade angle. The 20-inch nacelles; 0.40c propeller location; C_L, 0.25; cowling closed.

Figure 31.- Variation of propulsive efficiency with blade angle. The 20-inch nacelles; 0.25c propeller location; C_L, 0.25; cowling closed.

Figure 32.- Variation of propulsive efficiency with blade angle. The 10.4-inch nacelles; 0.40c propeller location; C_L, 0.25; cowling closed.

Figure 33.- Variation of propulsive efficiency with blade angle. The 10.4-inch nacelles; 0.25c propeller location; C_L, 0.25; cowling closed.

Figure 34.- Variation of propulsive efficiency with lift coefficient. The 20-inch nacelles; 0.40c propeller location; β, $23\frac{1}{2}^\circ$; air flowing through cowling.

Figure 35.- Variation of propulsive efficiency with lift coefficient. The 20-inch nacelles; 0.25c propeller location; β, $23\frac{1}{2}^\circ$; air flowing through cowling.

Figure 36.- Variation of propulsive efficiency with lift coefficient. The 10.4-inch nacelles; 0.40c propeller location; β, $23\frac{1}{2}^\circ$; air flowing through cowling.

Figure 37.- Variation of propulsive efficiency with lift coefficient. The 10.4-inch nacelles; 0.25c propeller location; β, $23\frac{1}{2}^{\circ}$; air flowing through cowling.

Figure 38.- Variation of maximum over-all efficiency with nacelle size. The 0.25c propeller location; C_L, 0.25; β, approximately 30°; air flowing through cowling.

Figure 39.- Variation of maximum over-all efficiency with lift coefficient. Various nacelle arrangements; β, $23\frac{1}{2}^{\circ}$.

Figure 40.- Effect of propeller operation on lift coefficient of the model for various index thrust coefficients. The 20-inch nacelles; 0.40c propeller location.

Figure 41.- Effect of propeller operation on lift coefficient of the model for various index thrust coefficients. The 10.4-inch nacelles; 0.25c propeller location.

Figure 42.- Effect of propeller operation on lift coefficient of the model for various index thrust coefficients. The 7-inch nacelles; 0.13c propeller location.

Figure 43.- Variation of pitching-moment coefficient of the model with index thrust coefficient. The 20-inch nacelles; 0.40c propeller location.

Figure 44.- Variation of pitching-moment coefficient of the model with index thrust coefficient. The 10.4-inch nacelles; 0.25c propeller location.

Figure 45.- Variation of pitching-moment coefficient of the model with index thrust coefficient. The 7-inch nacelles; 0.13c propeller location.

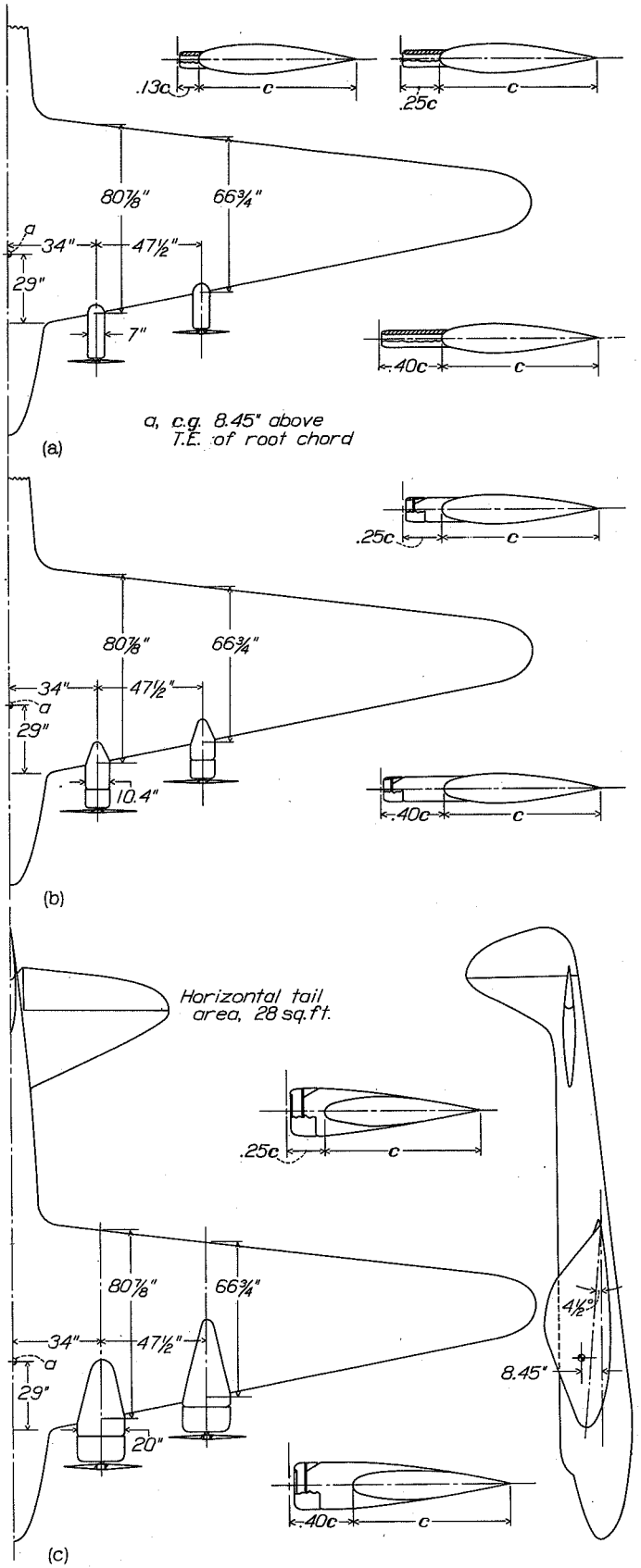
.13c
c
.25c
80 7/8"
66 3/4"
a
34"
47 1/2"
29"
7"
.40c
a, c.g. 8.45" above
T.E. of root chord
(a)
10.4"
(b)
Horizontal tail
area, 28 sq.ft.
4 1/2°
8.45"
20"
(c)

Figure 1.

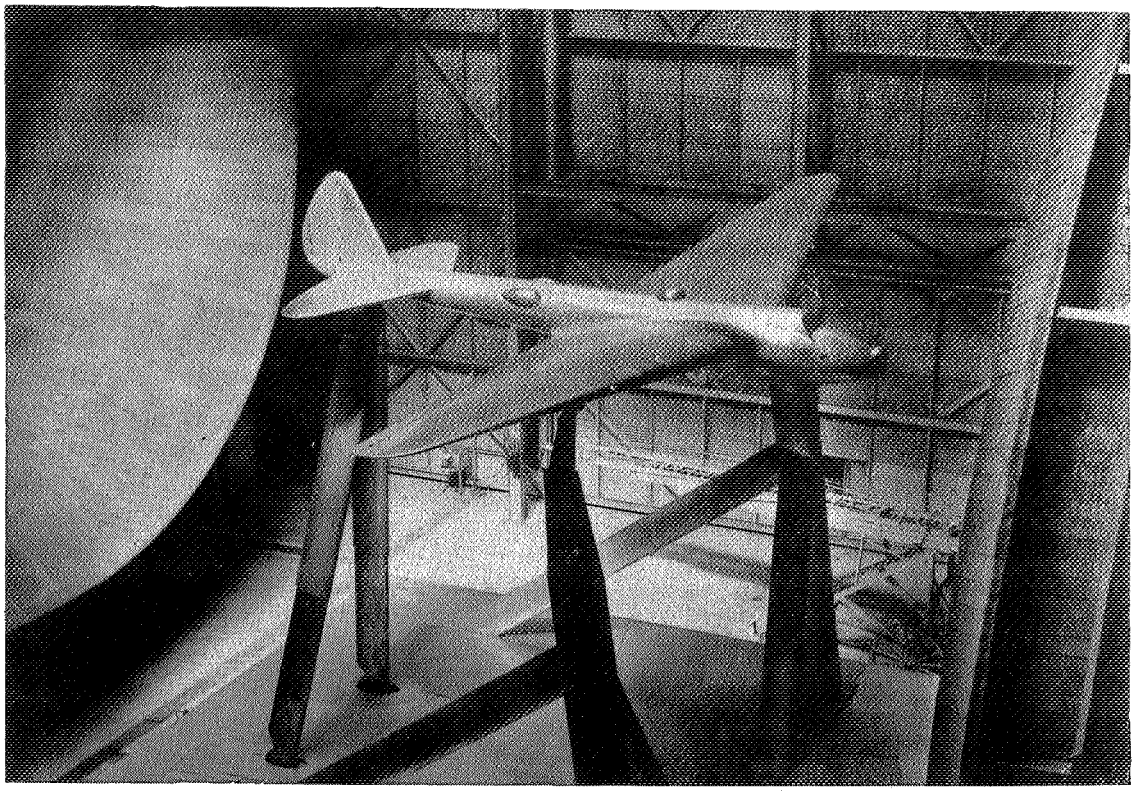

Figure 2.

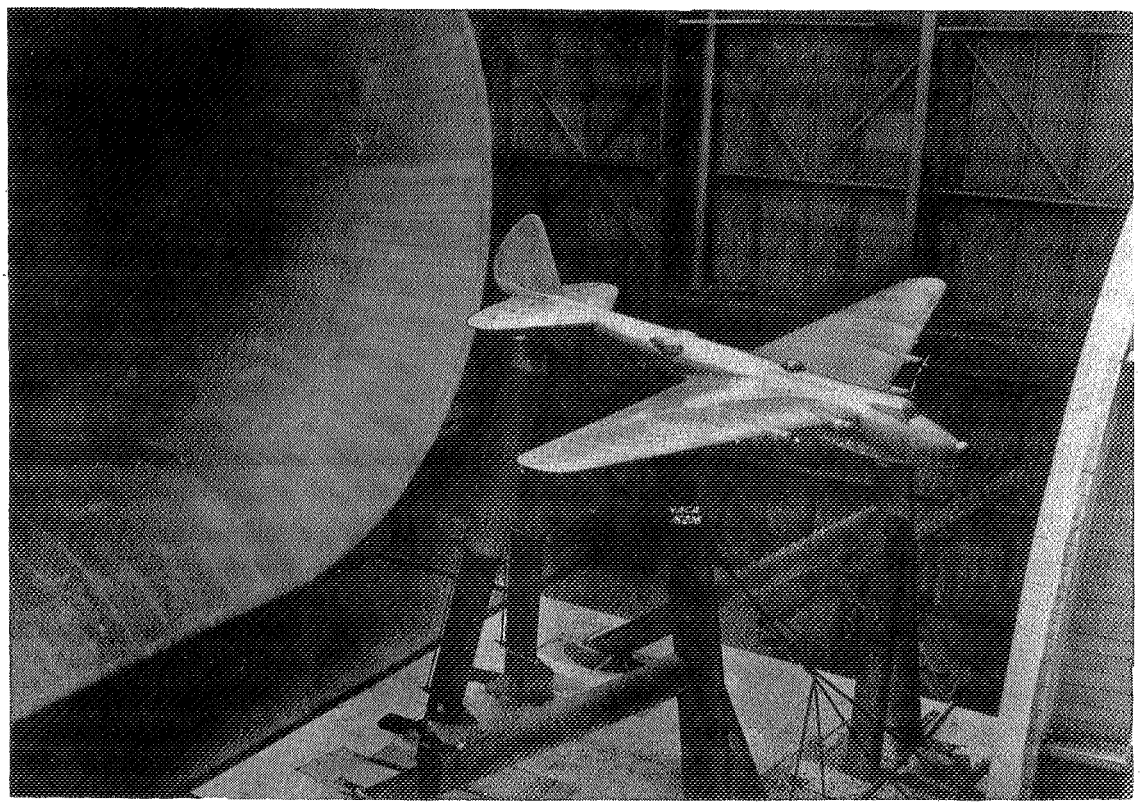

Figure 3.

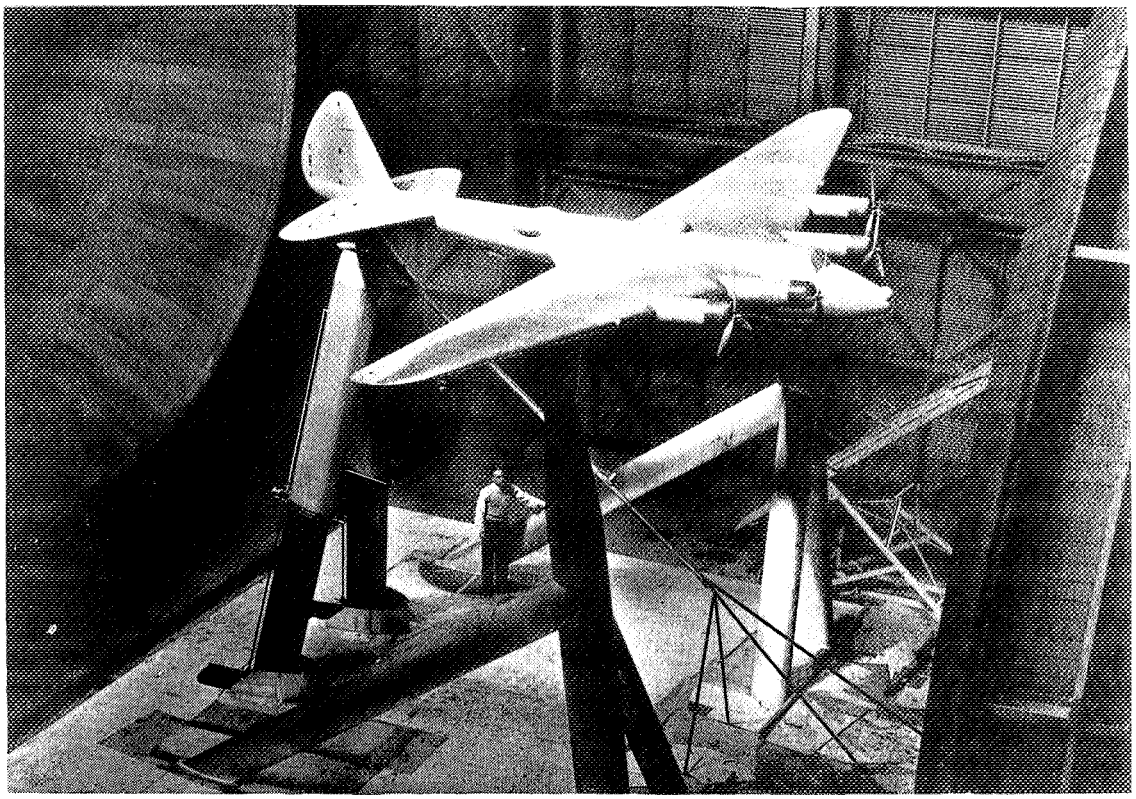

Figure 4.

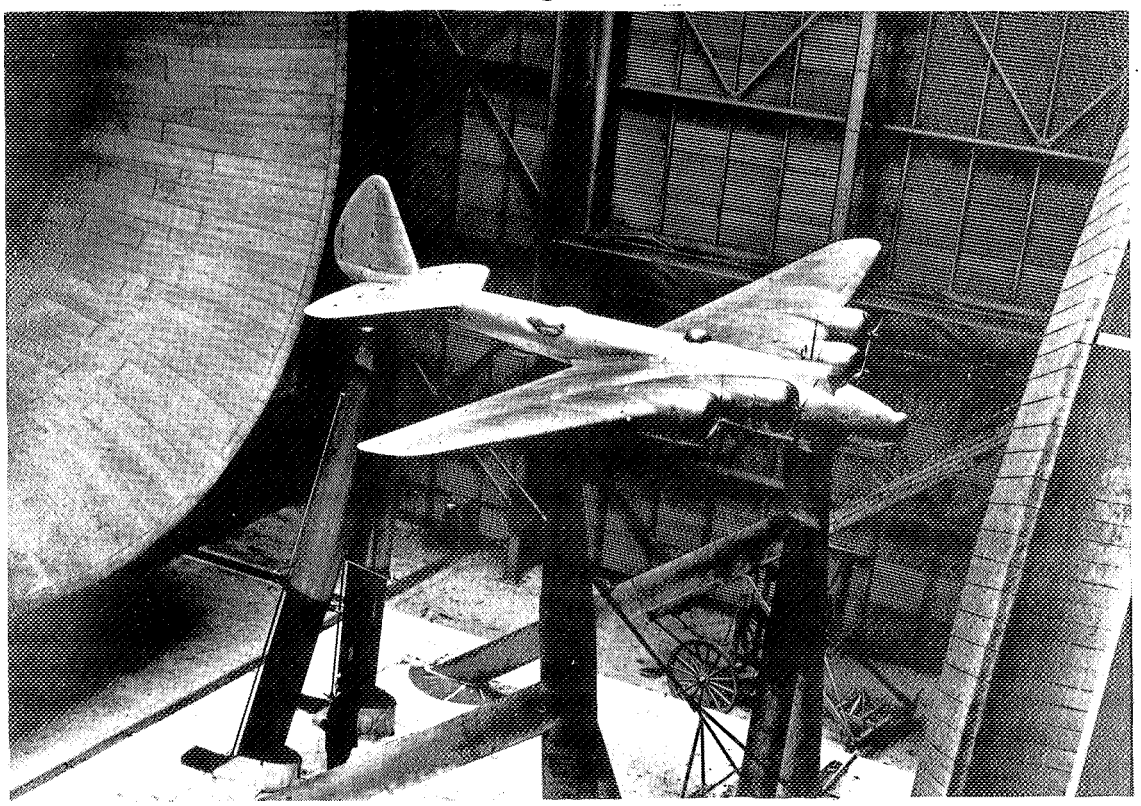

Figure 5.

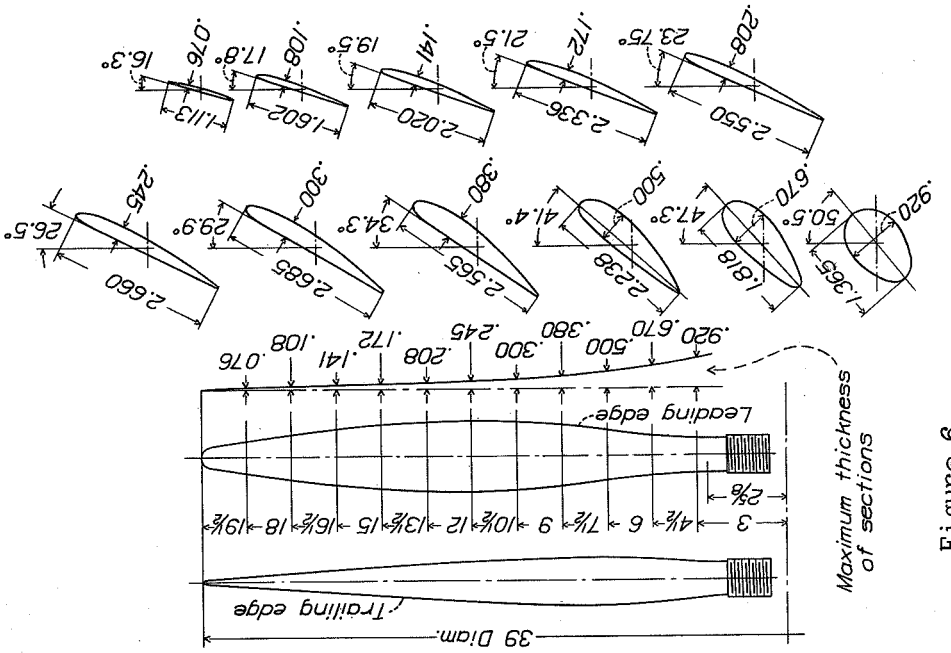

Figure 6.

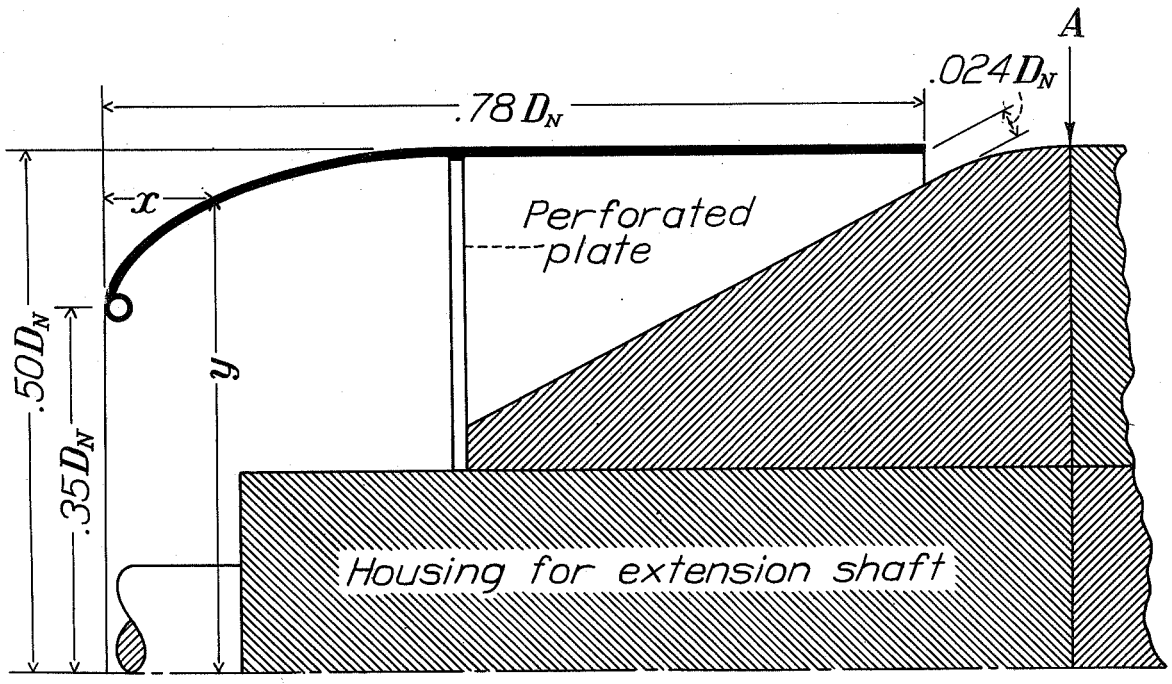

Figure 7.

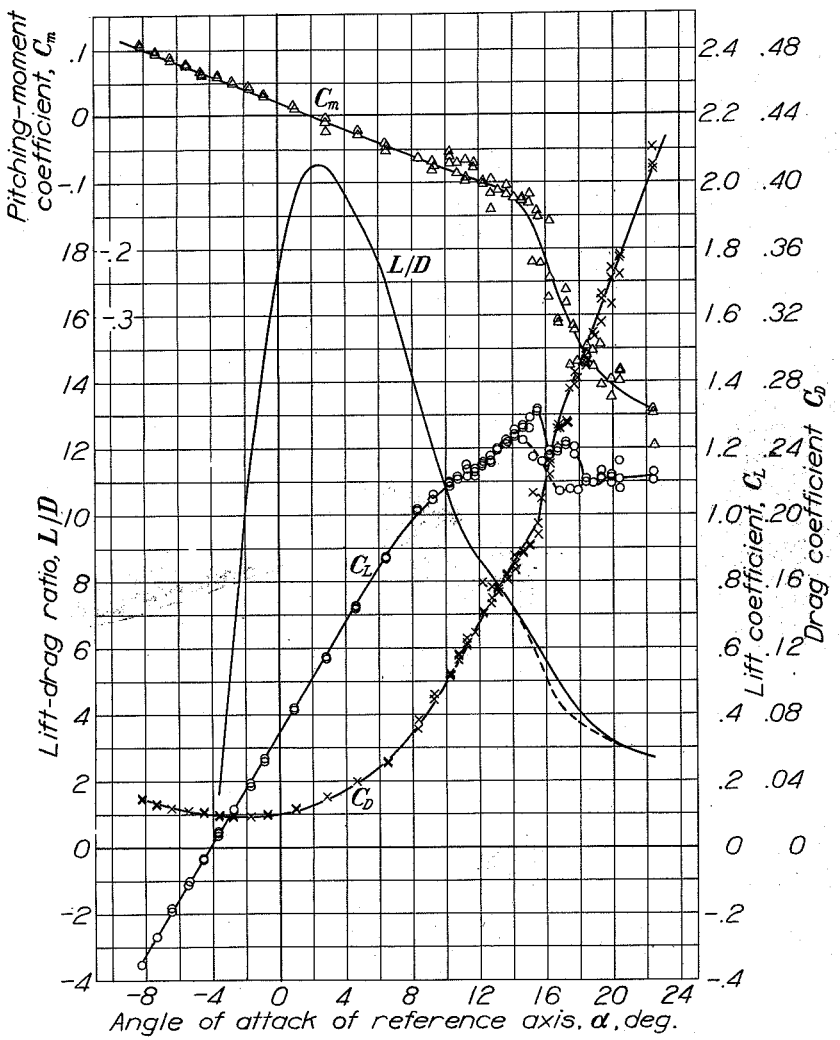

Figure 8

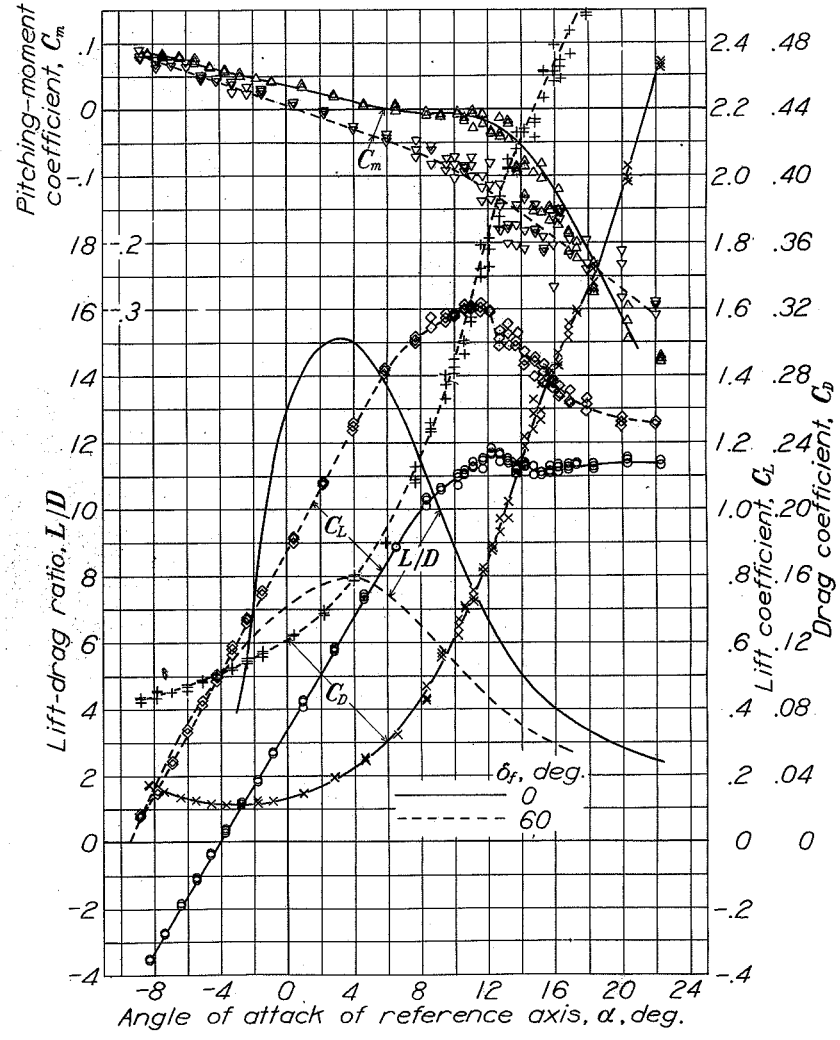

Figure 9

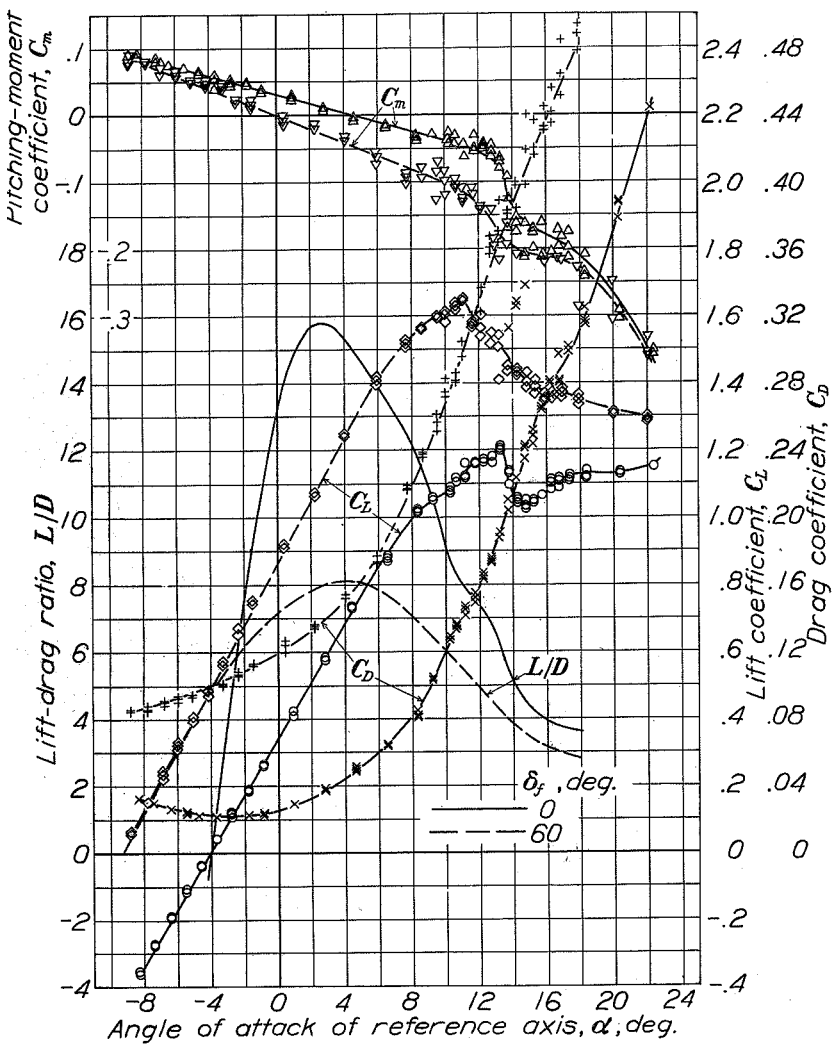

Figure 10

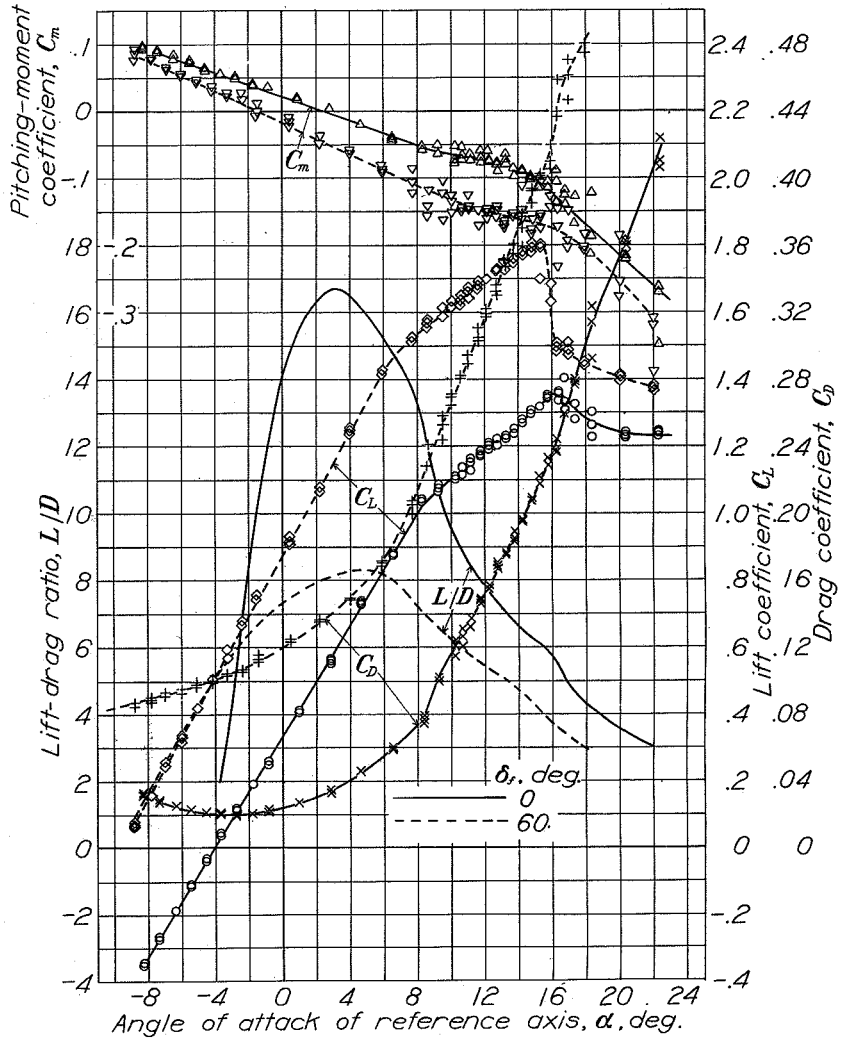

Figure 11

N.A.C.A.

Figs. 10,11

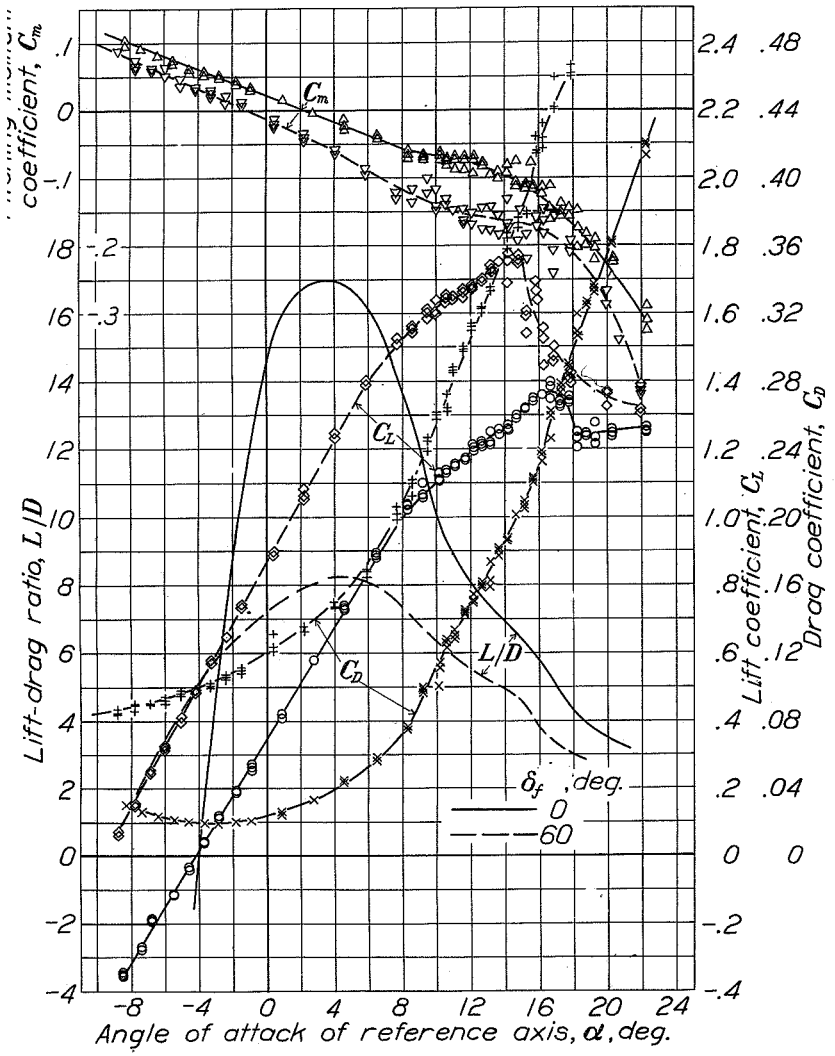

Figure 12

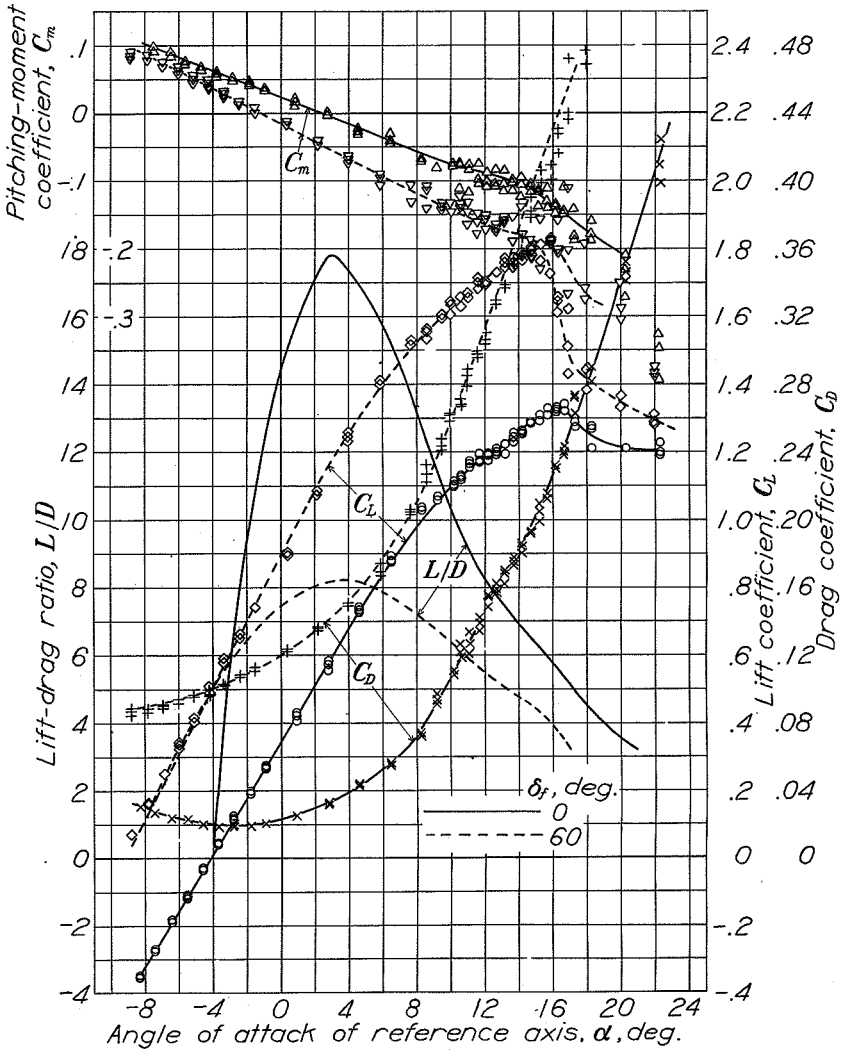

Figure 13

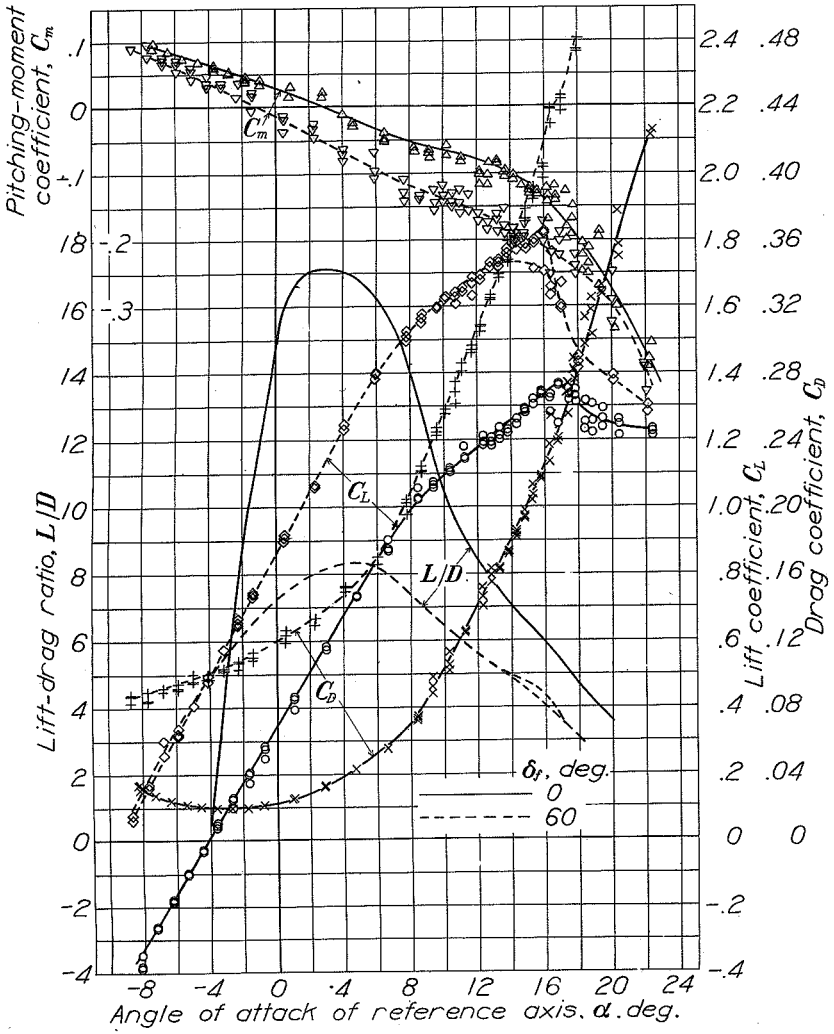

Figure 14

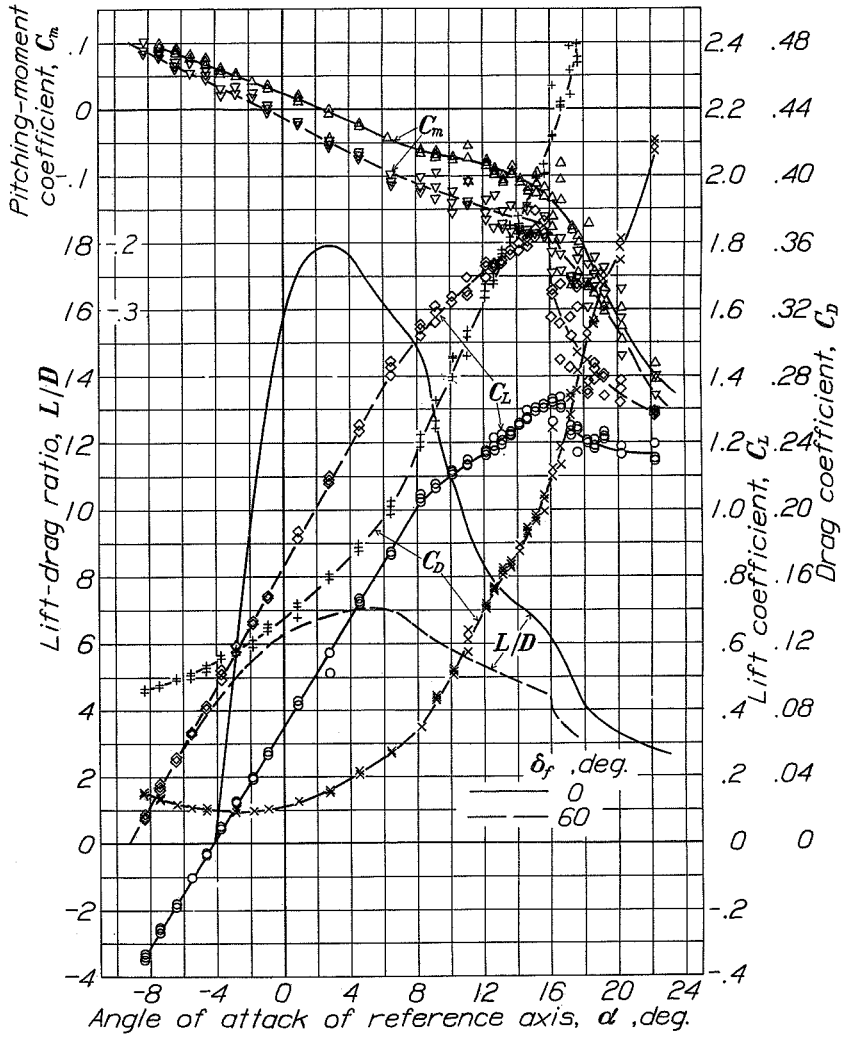

Figure 15

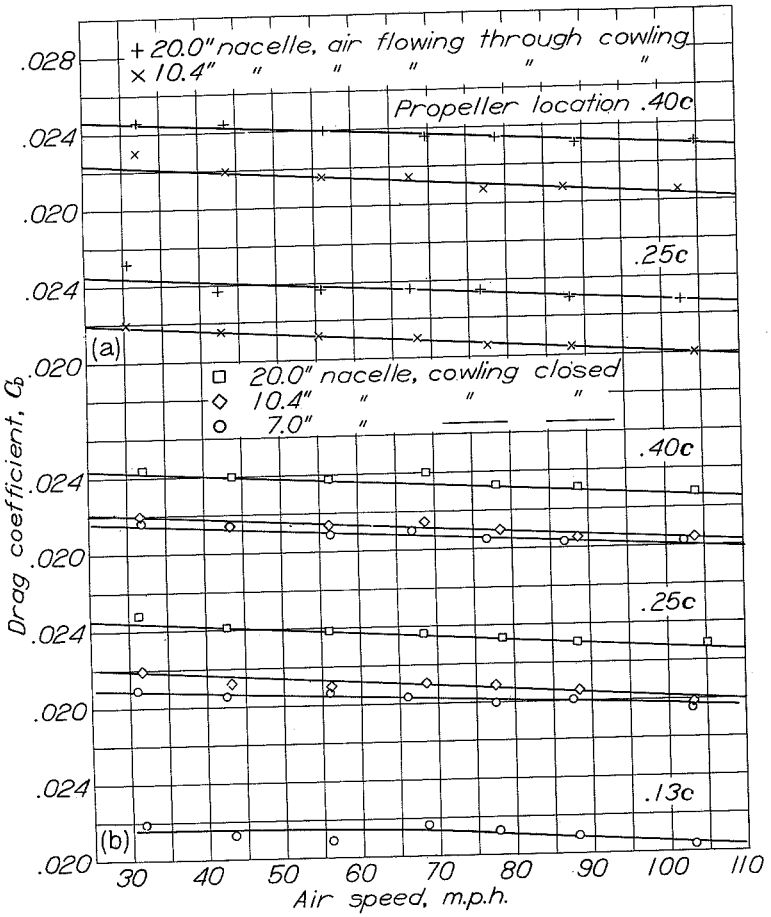

Figure 16.

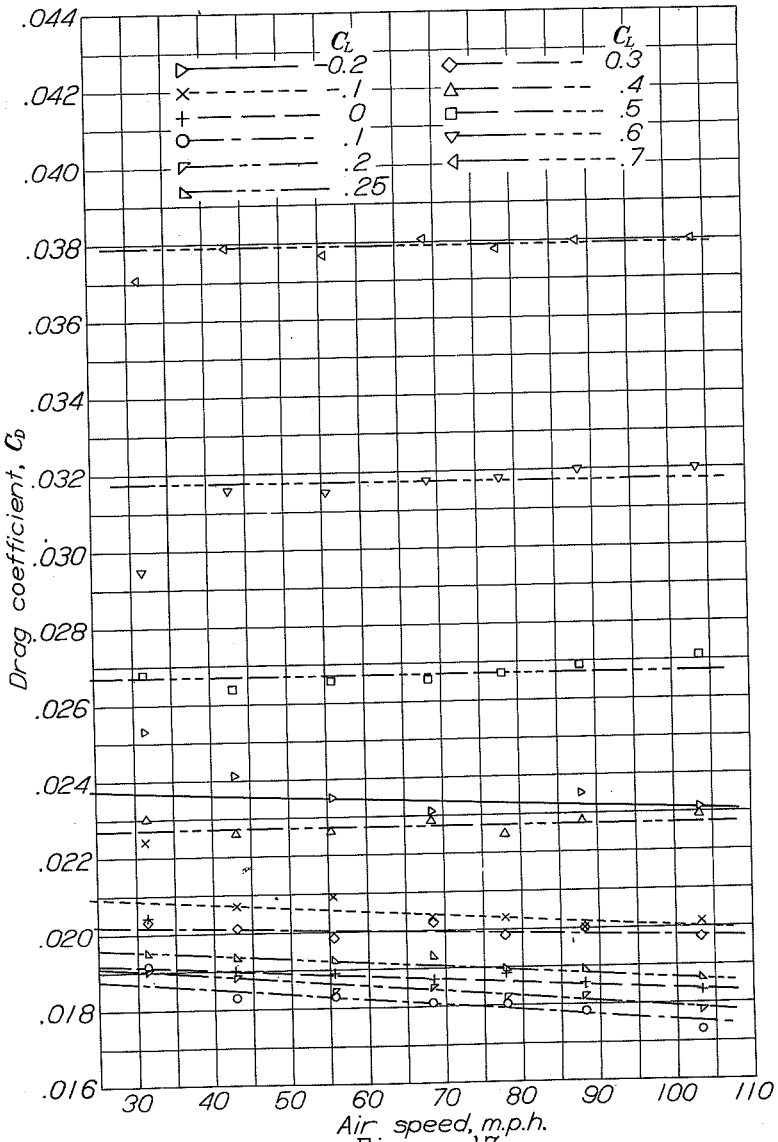

Figure 17

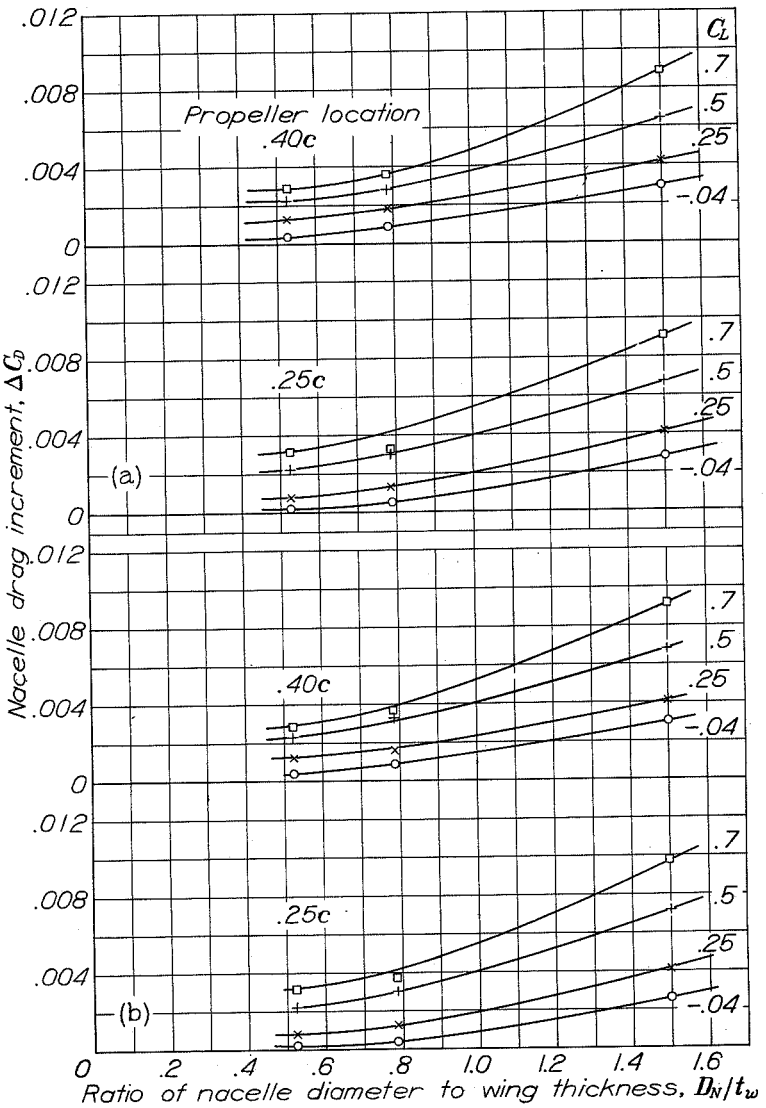
.012
.008
.004
0
Propeller location
.40c
.25c
(a)
(b)
C_L
.7
.5
.25
-.04
Nacelle drag increment, ΔC_D
0
.2
.4
.6
.8
1.0
1.2
1.4
1.6
Ratio of nacelle diameter to wing thickness, D_N/t_w

Figure 18.

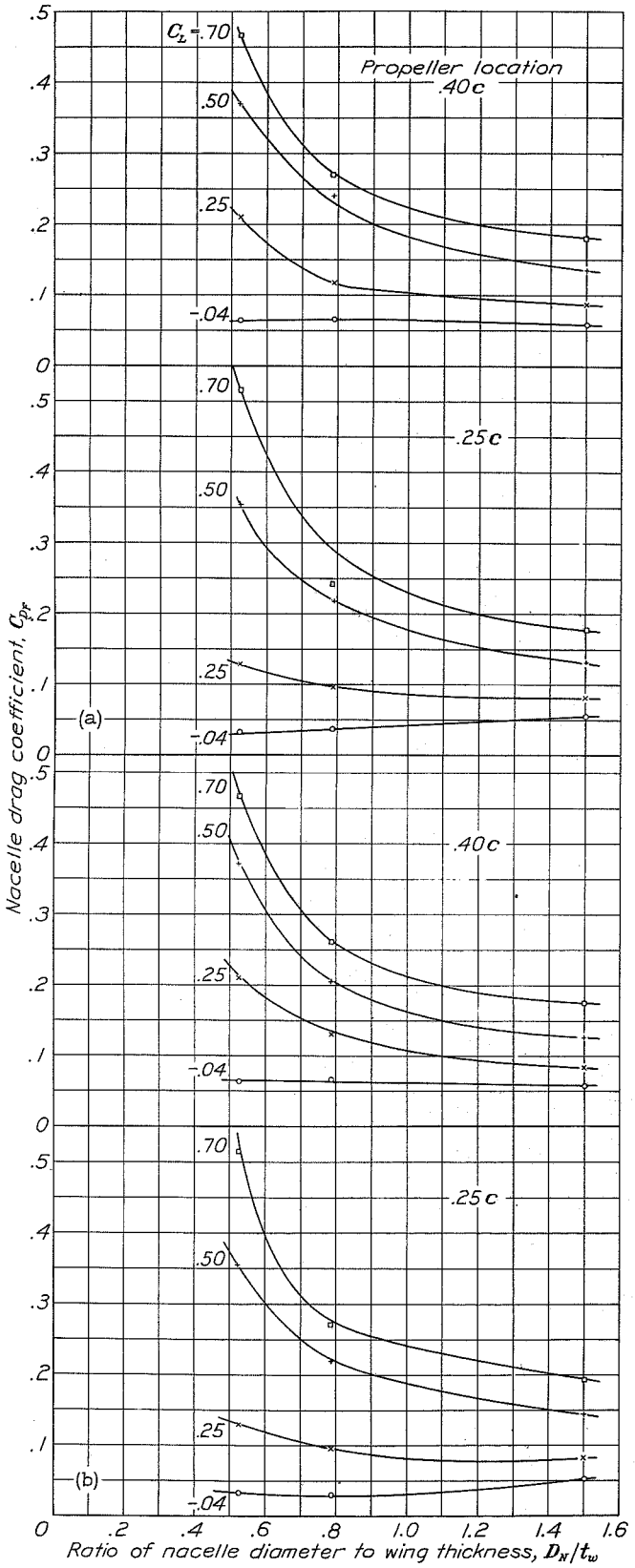

Figure 19.

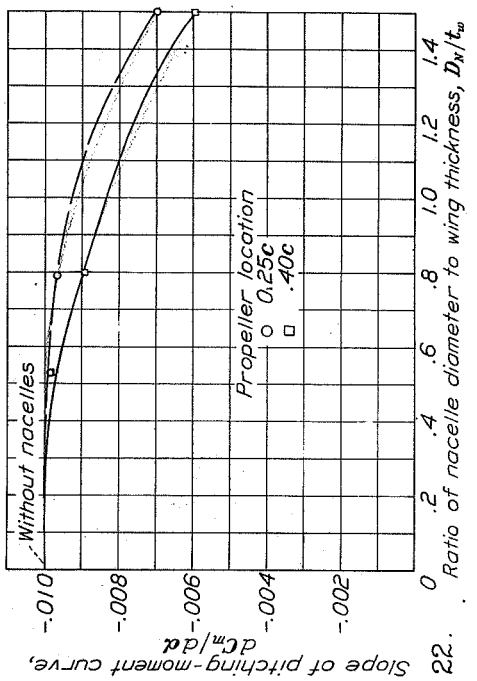

Figure 22.

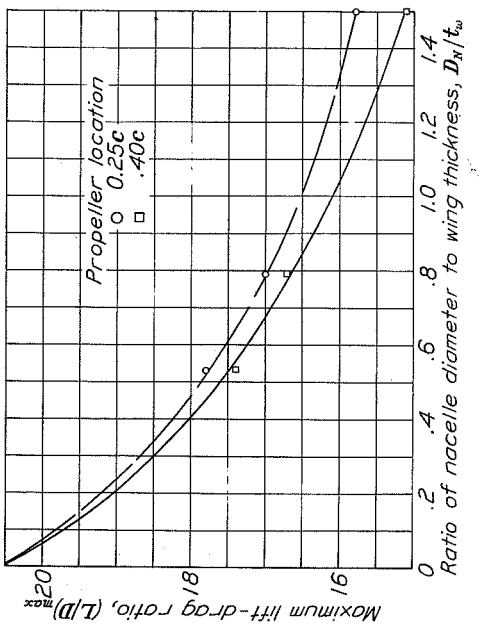

Figure 21.

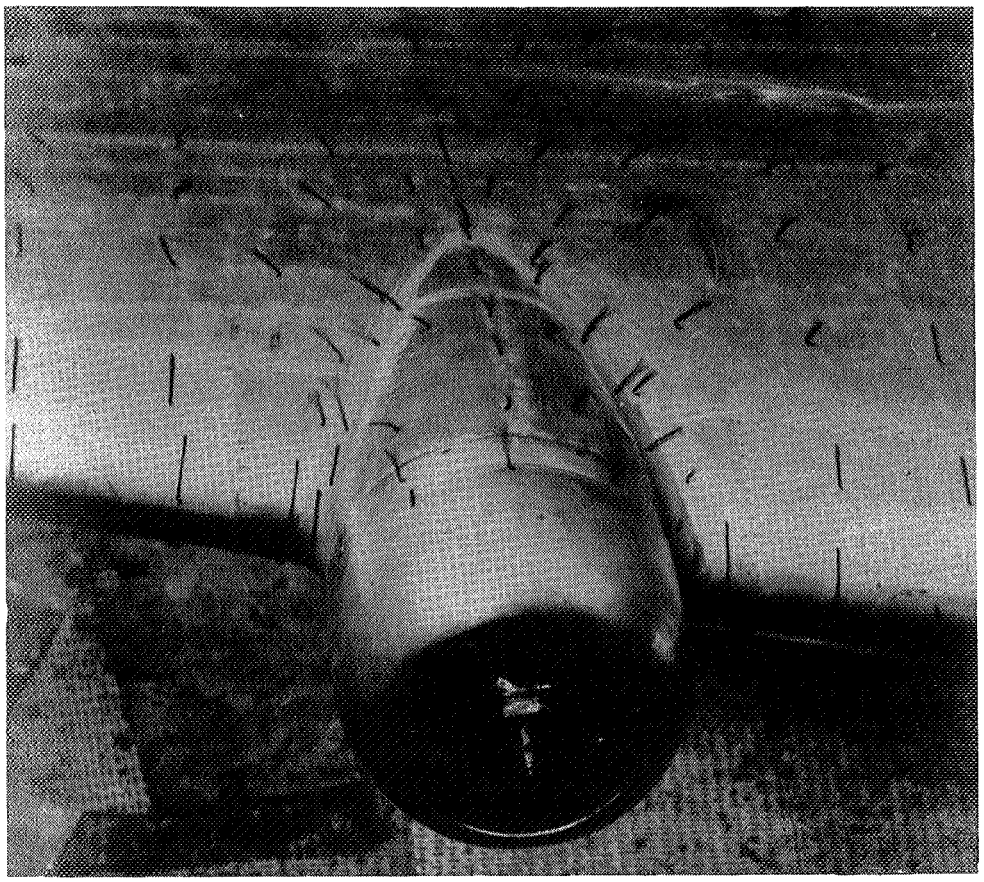

Figure 20.

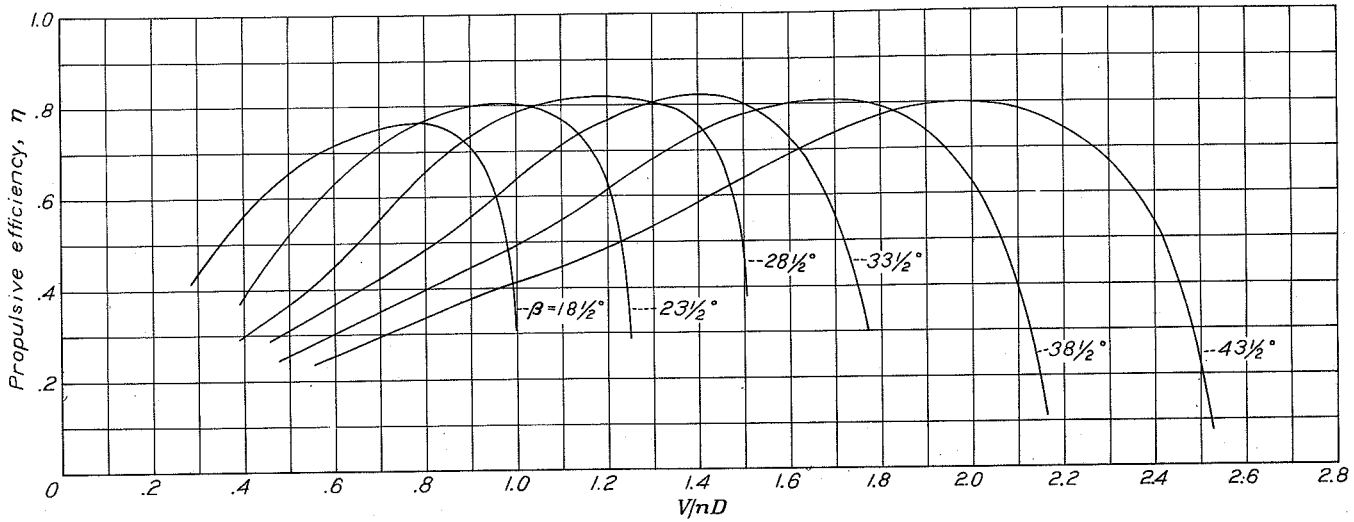

Figure 23.

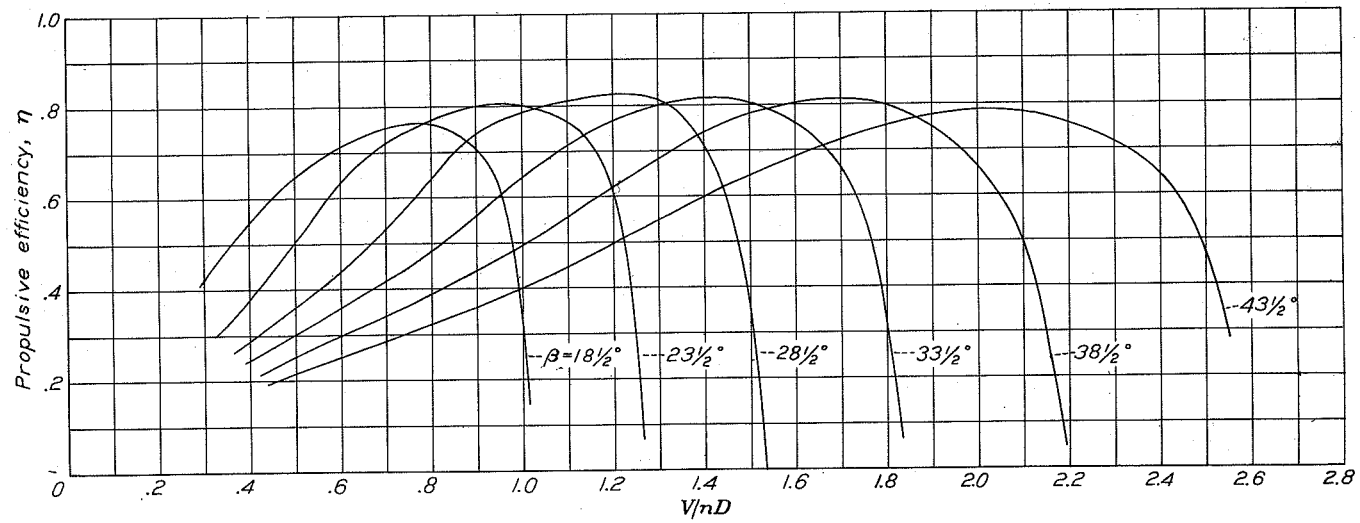

Figure 24.

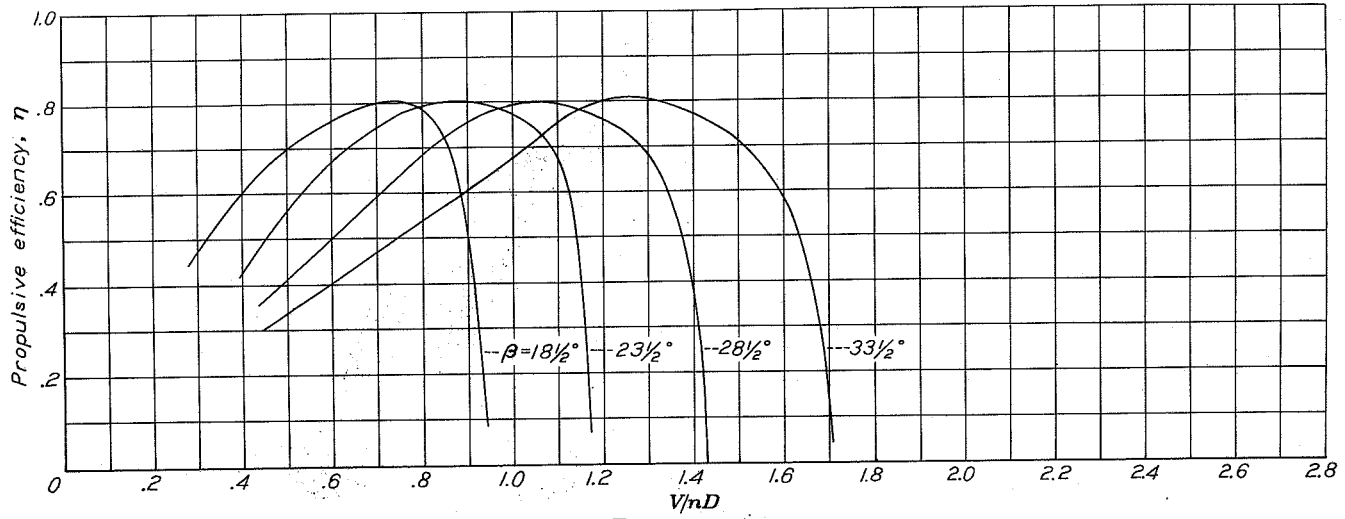

Figure 25.

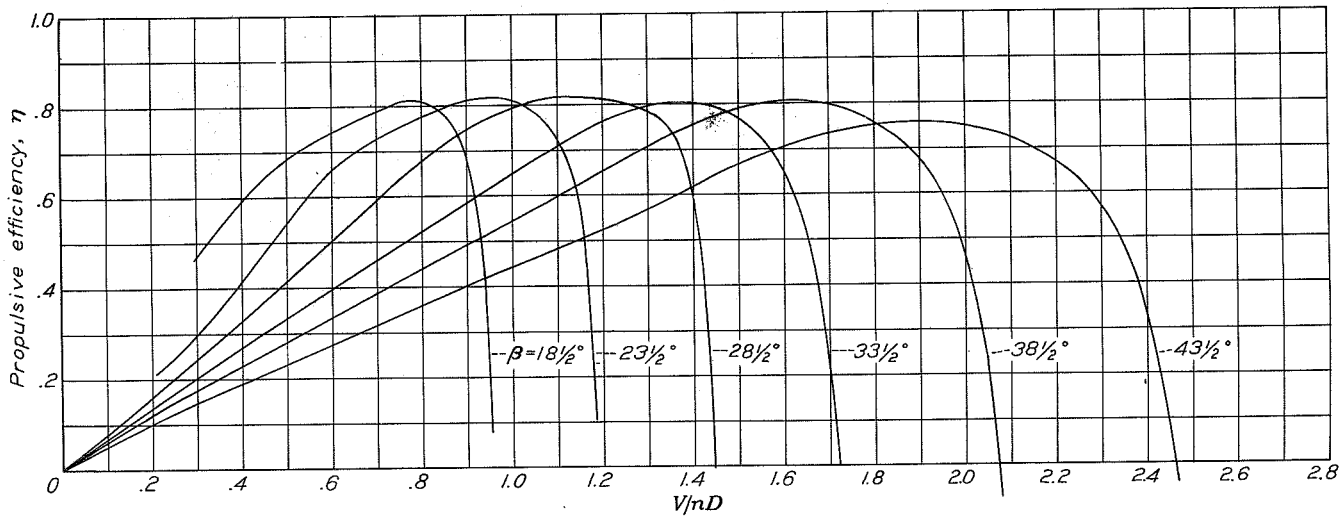

Figure 26.

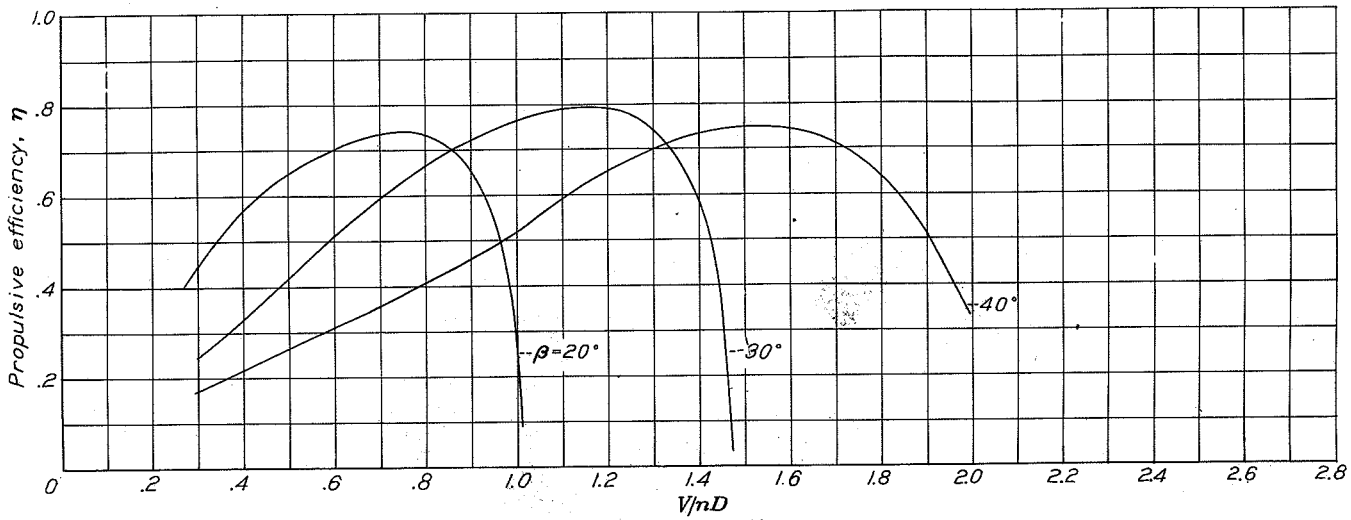

Figure 27.

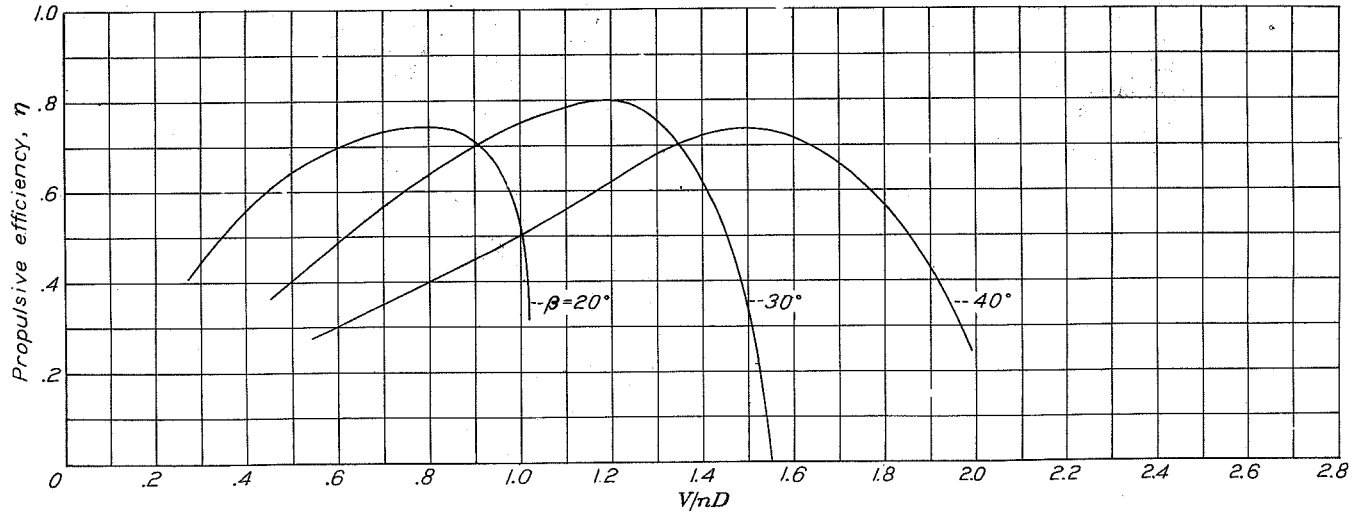

Figure 28.

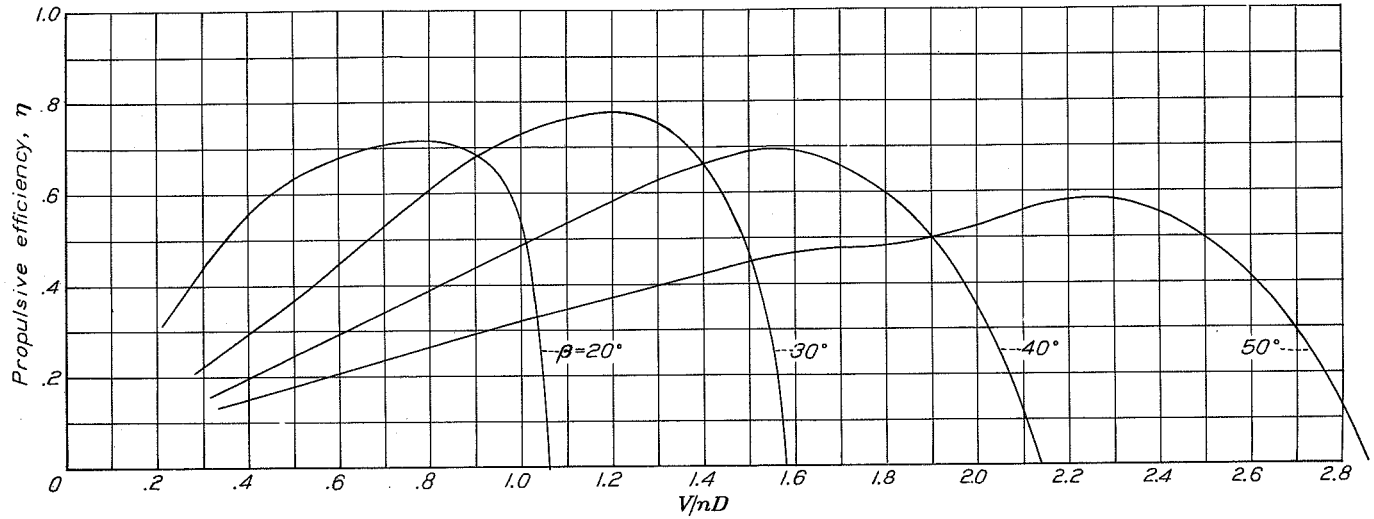

Figure 29.

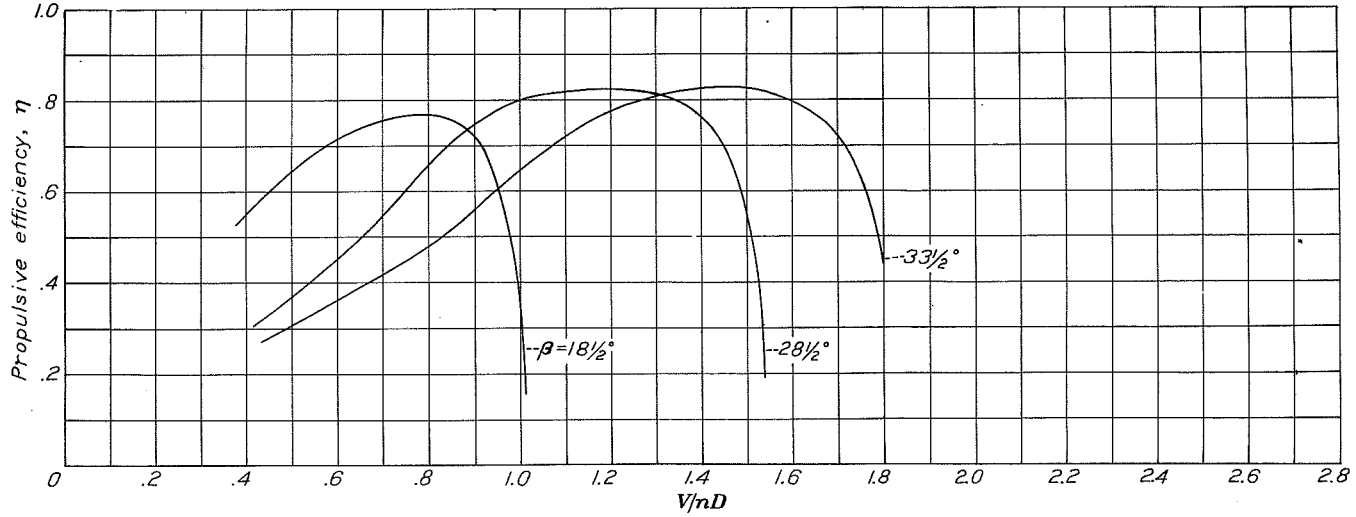

Figure 30.

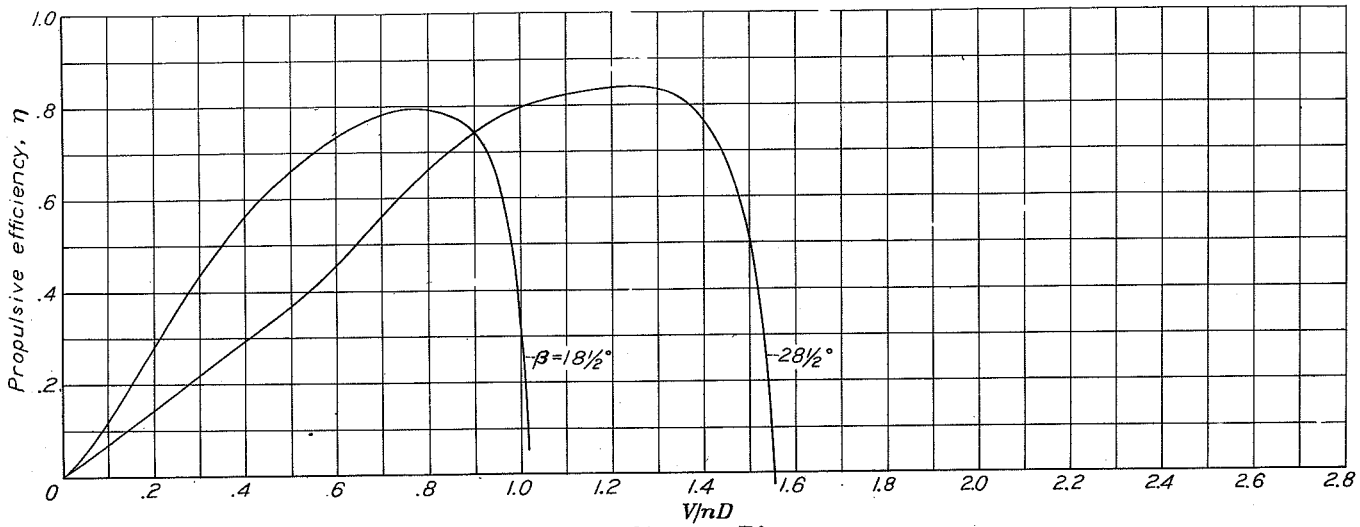

Figure 31.

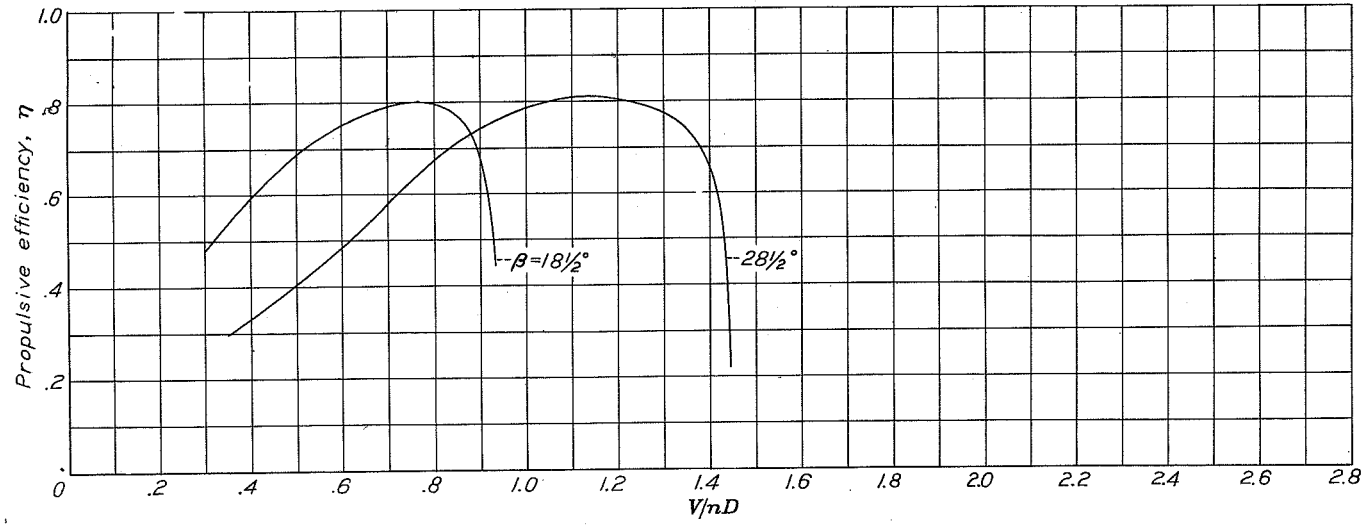

Figure 32.

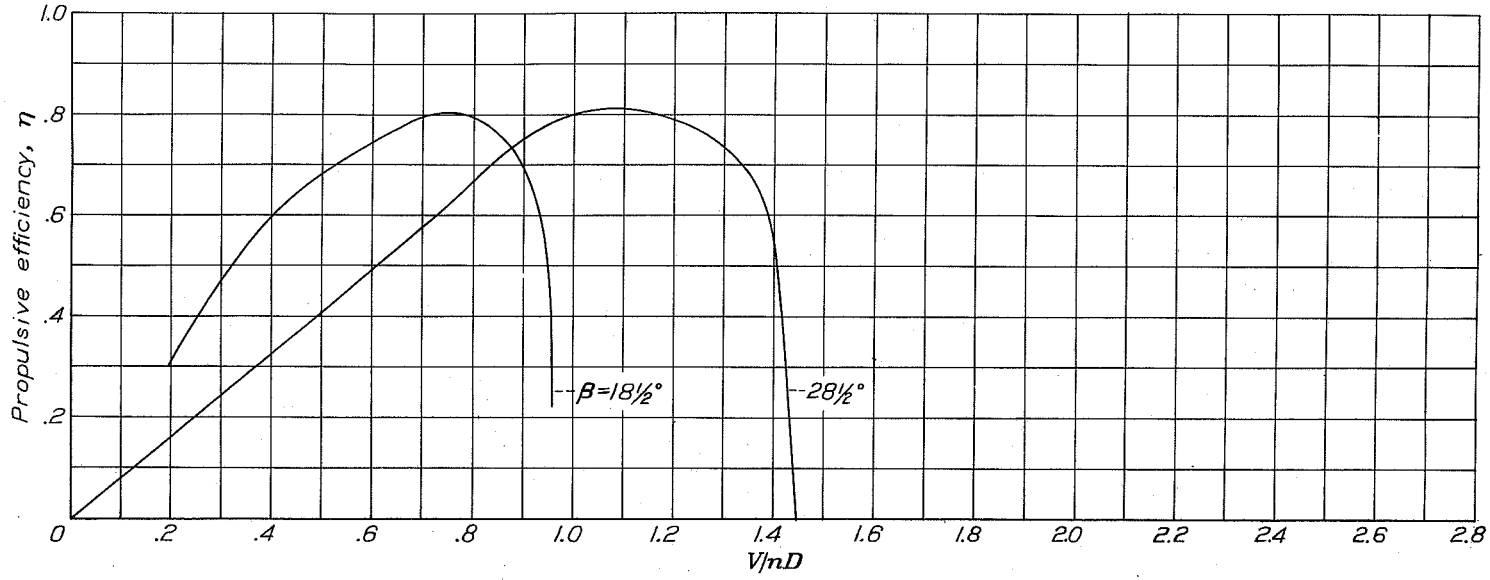

Figure 33.

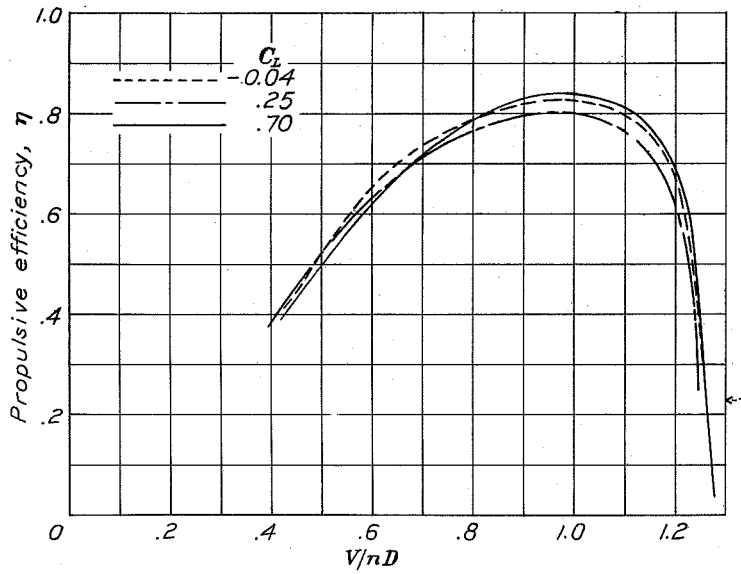

Figure 34.

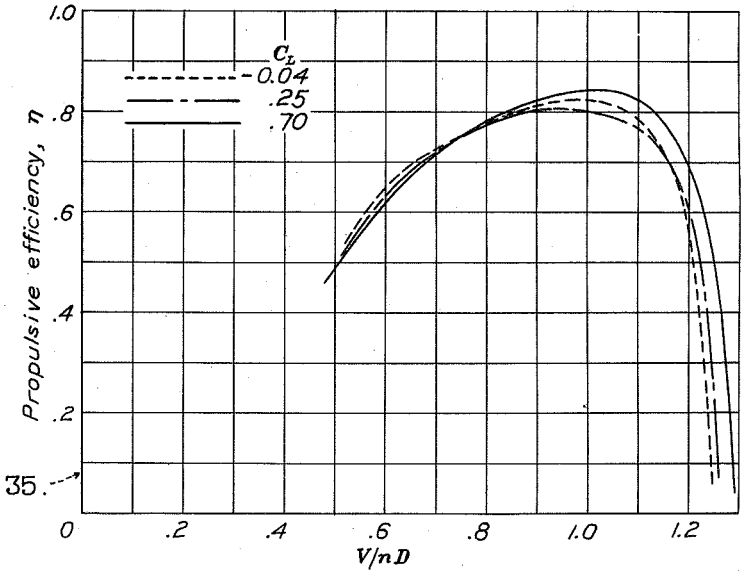

Figure 35.

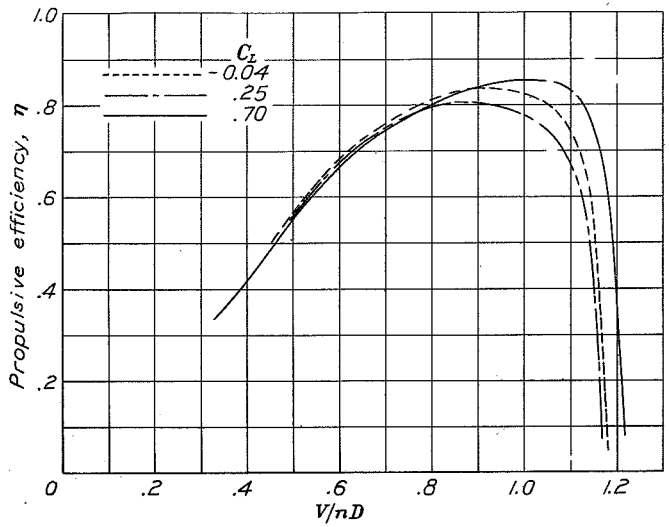

Figure 36.

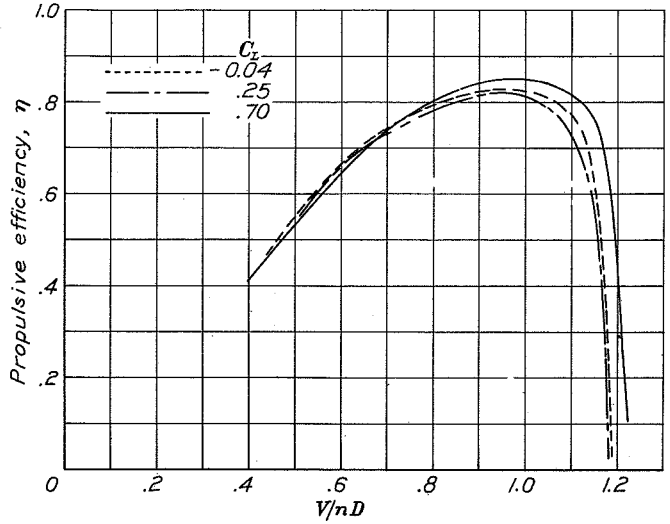

Figure 37.

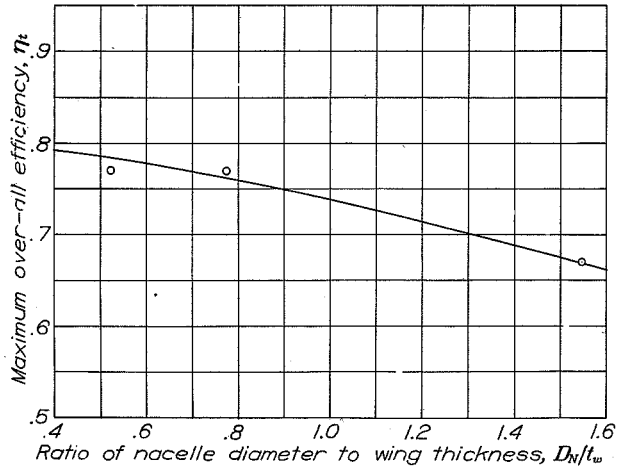

Figure 38.

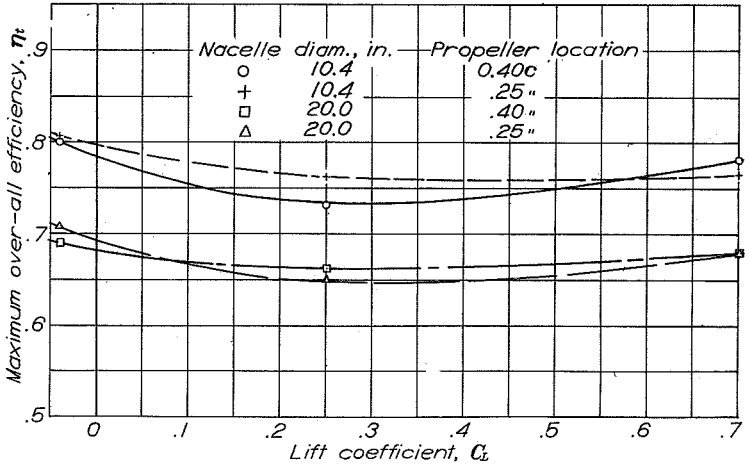

Figure 39.

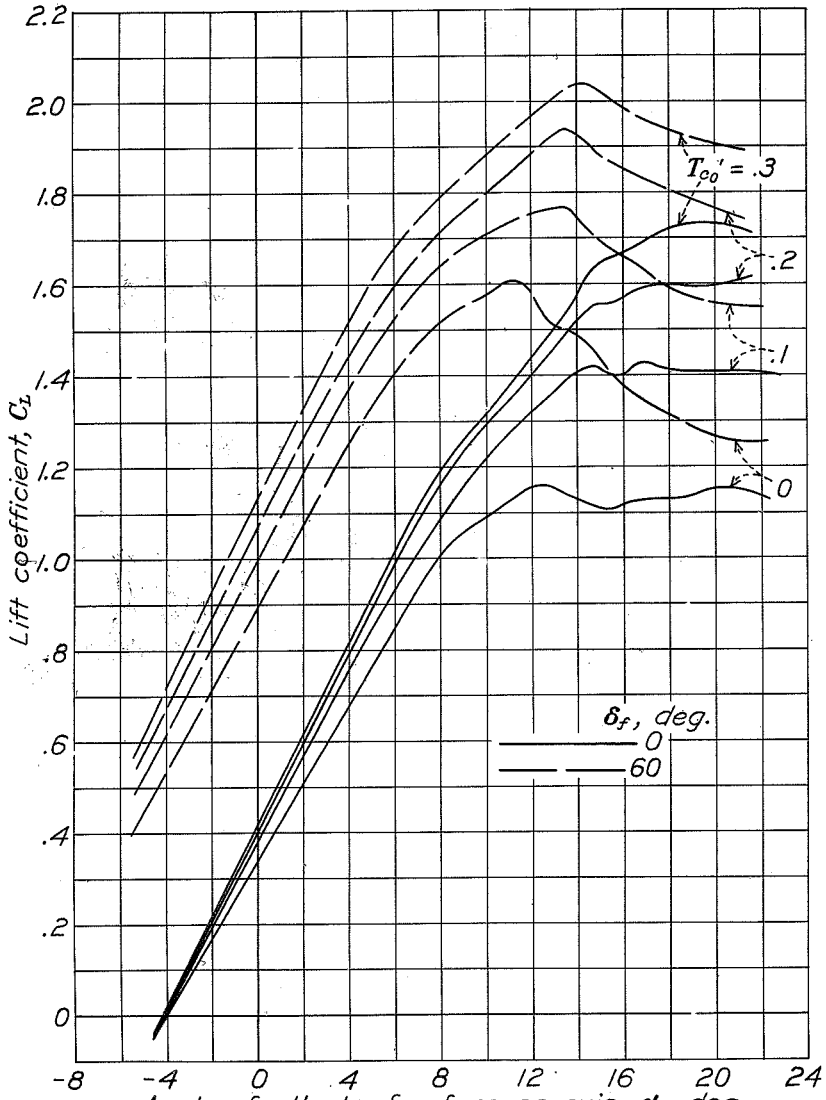

Figure 40.

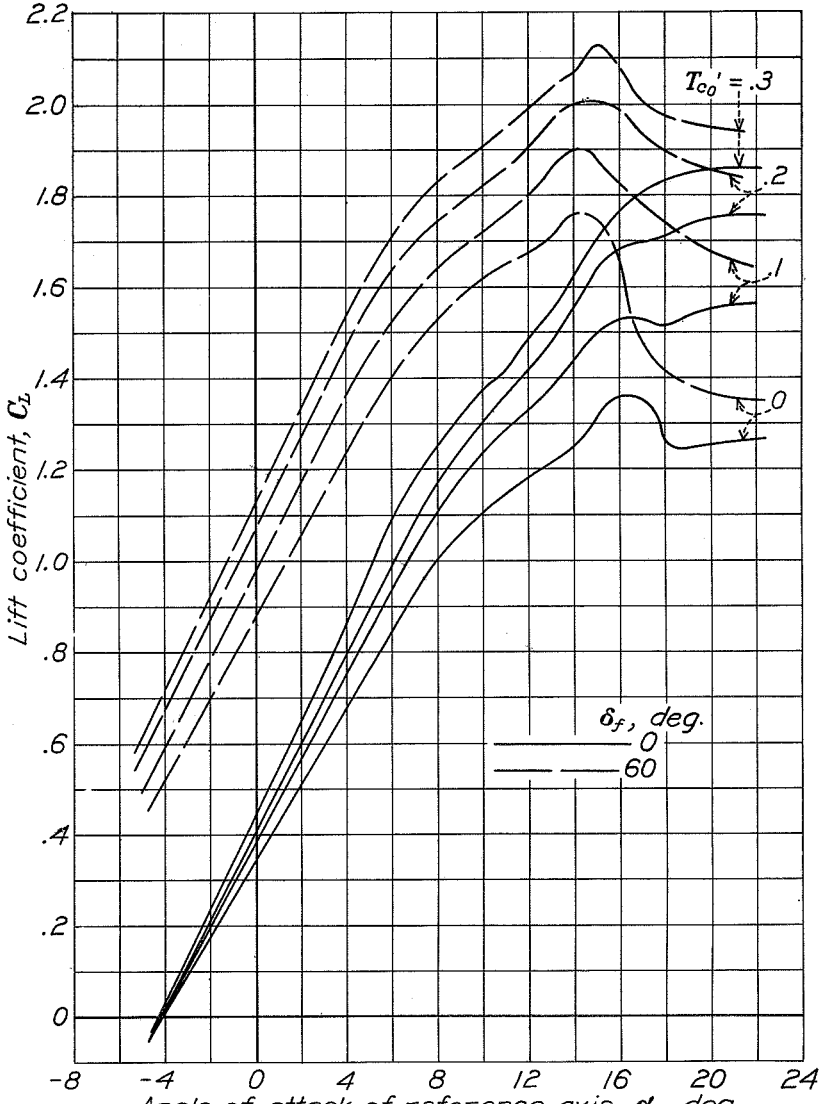

Figure 41.

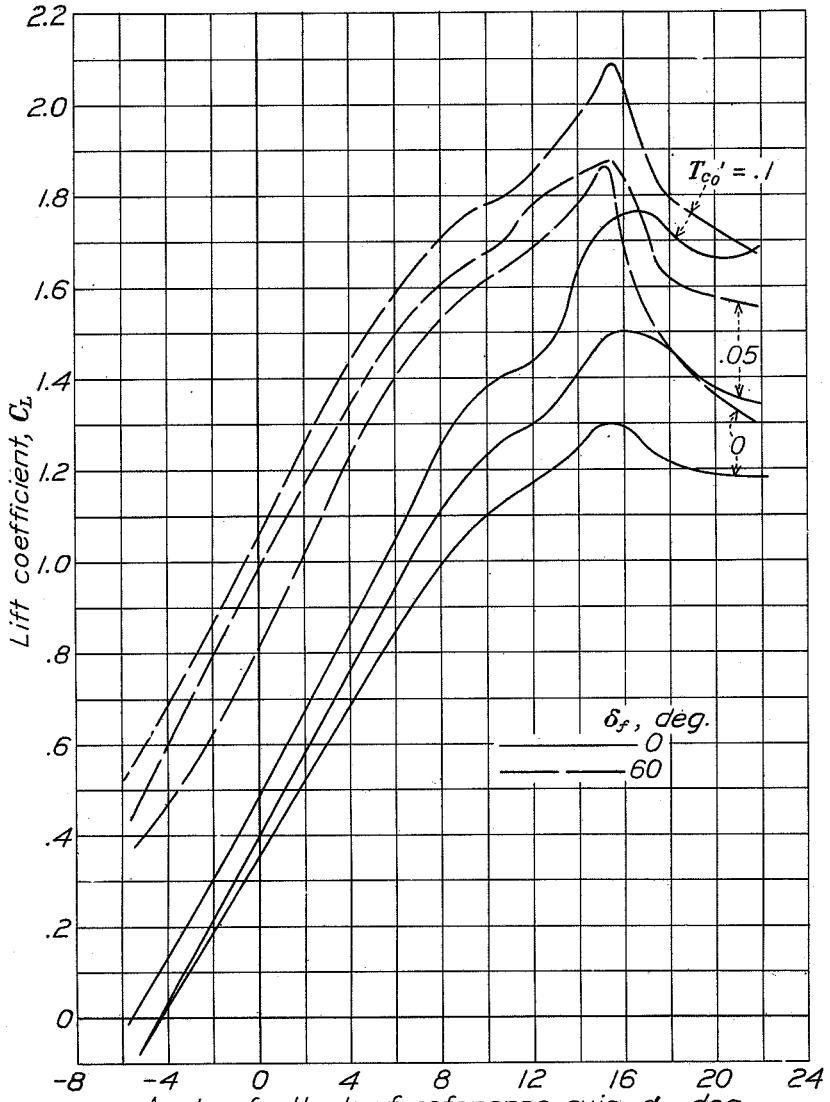

Figure 42.

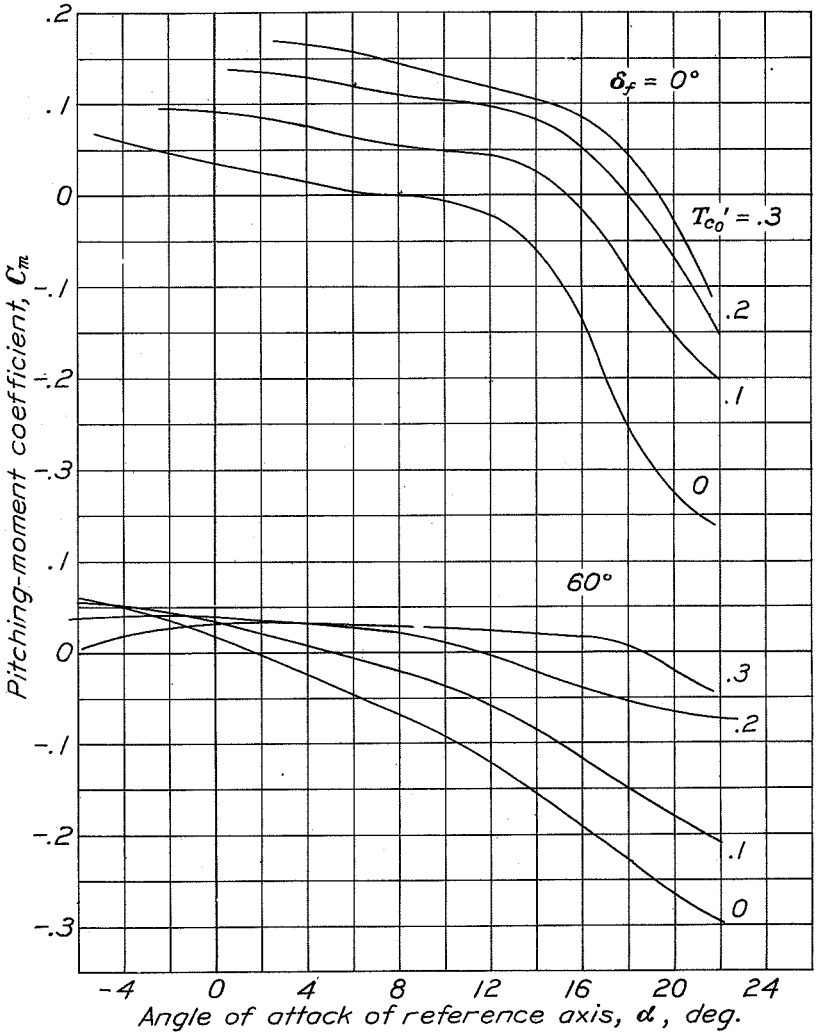

Figure 43.

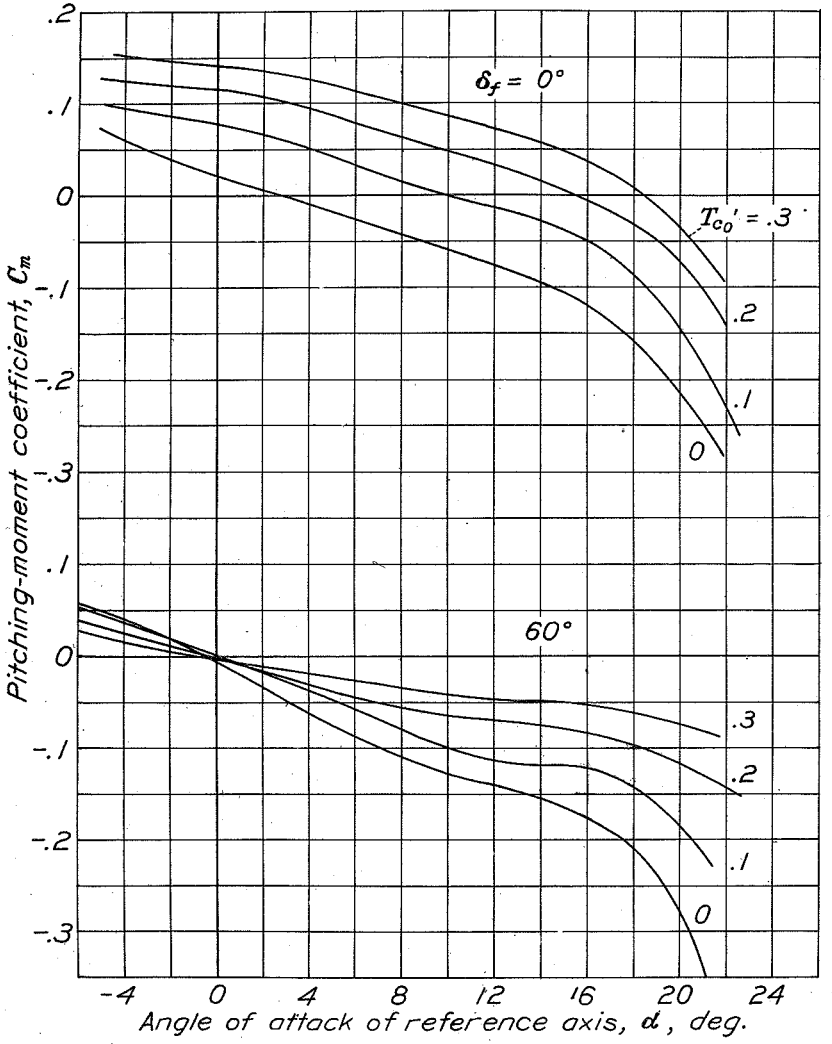

Figure 44.

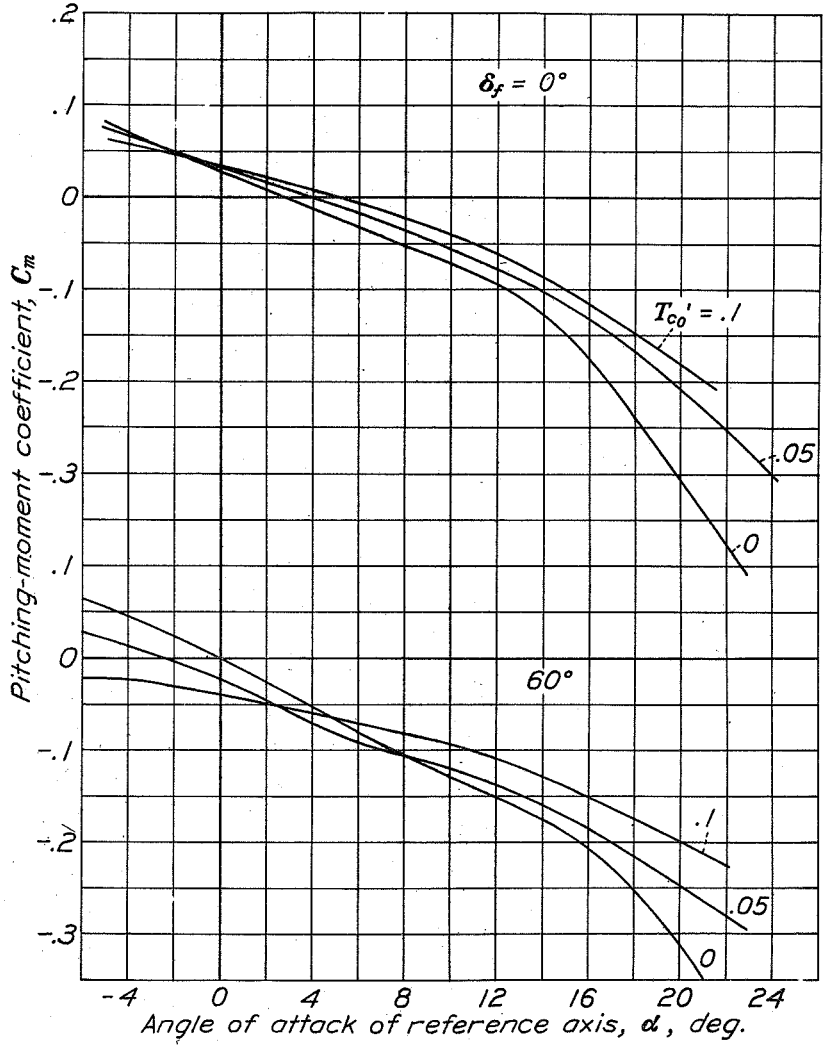

Figure 45.